



# Overview of Researches on the Nondestructive Testing Method of Metal Magnetic Memory: Status and Challenges

Pengpeng Shi<sup>1,2</sup> · Sanqing Su<sup>1</sup> · Zhenmao Chen<sup>2</sup>

Received: 14 October 2019 / Accepted: 23 May 2020 / Published online: 31 May 2020  
© Springer Science+Business Media, LLC, part of Springer Nature 2020

## Abstract

More than 20 years of research progress regarding the nondestructive testing method of metal magnetic memory is reviewed and summarized in detail. Consequently, this overview is selective, covering what we feel are the most important trends of experimental phenomena, mechanism explanations, quantitative theories, simulations, testing, evaluation and application. From analyzing the current state of research on the method of metal magnetic memory, some key problems and future developmental trends are proposed. Although the research on magnetic memory method has made great progress, the practical application still faces problems such as complex influencing factors and less quantitative research. In the future, for magnetic memory method, it is necessary to strengthen the microscopic observations of magnetic domains, experiments of magnetomechanical constitutive, establishment of quantitative models, modeling of complex influencing factors, and the study of identification, inversion and criteria. In addition, the combination of other non-destructive testing methods can greatly improve the practical application of the magnetic memory method.

**Keywords** Metal magnetic memory · Mechanism · Theory · Simulation · Experiment

## 1 Introduction

Ferromagnetic materials represented by steel have good mechanical properties, and engineering structures made from them are used widely in aerospace, railways, pipelines, pressure vessels, and the petrochemical industry. However, because of either the level of preparation process or fatigue during use, the damage that forms in ferromagnetic materials has a direct effect on the service safety of engineering structures and can even cause catastrophic accidents. In engineering applications, the location and degree of damage

in an engineering structure must be determined in a timely manner, whereupon measures such as grinding, welding, and replacement must be taken to avoid an accident due to material damage. Nondestructive testing refers to the detection of damage without affecting the performance of the structure or material, and for many industries the nondestructive testing of ferromagnetic materials is very important both theoretically and practically [1–5].

The relationship between the magnetic properties of ferromagnetic materials and the stress and damage therein has long been a research focus. Experimental studies have shown that the residual magnetization at welds in ferromagnetic materials is closely related to the magnitude of the residual stress [6]. Furthermore, Atherton et al. [7, 8] showed that changes in the magnetic field around a buried pipeline can reflect changes in the stress state of the pipeline. This means that the distribution of the magnetic signal is related to the stress state of the material, thereby making it possible to evaluate the stress state of a ferromagnetic material by using its magnetic signal [9]. It is worth pointing out that for the earlier studies [7, 8] mentioned above, the magnetic signal was measured with a relatively large lift-off distance.

The method of evaluating material stress and damage based on the self-magnetization field measured near

---

✉ Pengpeng Shi  
shipengpeng@mail.xjtu.edu.cn

✉ Zhenmao Chen  
chenzm@mail.xjtu.edu.cn

<sup>1</sup> School of Civil Engineering & Institute of Mechanics and Technology, Xi'an University of Architecture and Technology, Xi'an 710055, Shaanxi, People's Republic of China

<sup>2</sup> State Key Laboratory for Strength and Vibration of Mechanical Structures, Shaanxi Engineering Research Center of NDT and Structural Integrity Evaluation, Xi'an Jiaotong University, Xi'an 710049, Shaanxi, People's Republic of China

the surface is called the metal magnetic memory (MMM) method proposed by Doubov [10]. If the magnetic signal is measured near the material surface with small lift-off under the geomagnetic environment, the measured signal can be used to evaluate the stress concentration state and damage degree of the specimen near the measurement position. For example, the magnetic domain in the stress concentration zone can be regularly oriented because of the high load and geomagnetic field, and the self-magnetization field measured near the surface can be reserved even if the load is released. The MMM signal has some basic characteristics. As shown in Fig. 1 [11], the MMM signal near the defect or stress concentration has obvious non-linear characteristics. The tangential component  $H_x$  has a maximum value near the position of the stress concentration or defect zone, where the normal component  $H_y$  is usually equal to 0. Therefore, the location of the stress concentration or defect zone can be identified using the position of the maximum value of the tangential component  $H_x$  and the zero-value characteristic of the normal component  $H_y$ . In addition, the signal characteristics such as the peak-to-valley interval of the normal component  $H_y$  and the peak value of the tangential component  $H_x$  are related to the size of defect or stress concentration. This means that the measurement of the signal characteristics can theoretically quantify the size of the damage.

The MMM method is regarded as being a new nondestructive testing technology and is considered to be an effective NDT method for detecting early damage of ferromagnetic materials. The research to date on the mechanism and theory of the MMM method has involved the magnetomechanical coupling effect of ferromagnetic materials [11, 12], the basic characteristics of MMM signals induced by stress concentration and defects, and other basic issues related to the weak magnetic field and external forces. This series of

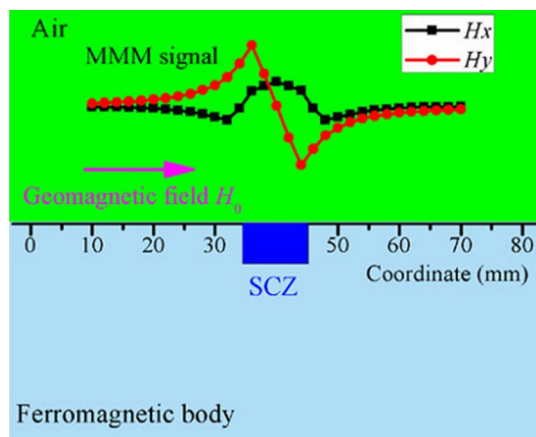


**Fig. 1** Schematic diagram of metal magnetic memory (MMM) signal caused by stress concentration zone (SCZ) [11], Copyright@2016, nondestructive testing and evaluation

studies helped to clarify the magnetomechanical behavior of ferromagnetic materials and enable quantitative evaluation of stress and damage based on the MMM method. In that way, the development of fatigue damage in ferromagnetic materials or structures in engineering applications can be monitored effectively. Research related to the MMM method is important both scientifically and for engineering applications. Such studies aid understanding of the damage phenomena and laws of ferromagnetic materials and contribute to the scientific determination of damage detection. Related research will also help resolve common scientific problems in the disciplines of mechanics and other sciences, such as multi-field coupling behavior and its applications.

The MMM method was proposed more than 20 years ago. Since then, there have been many studies and developments regarding the MMM method, but few comprehensive reviews [13–16]. The present paper introduces in detail the research progress that has been made since the MMM method was proposed, and it identifies some key issues to be addressed according to the current state of research. It is hoped that this review will allow more researchers to understand and enter this research field, thereby enabling the MMM method to better serve engineering applications and promoting the development of applied physics, ferromagnetics, mechanics, and nondestructive testing.

## 2 Basic Principle and Signal Characteristics

### 2.1 Basic Principle of Magnetomechanical Effect

Since 1997, Doubov and his colleagues proposed the NDT method known as the metal magnetic memory (MMM) method to detect stress concentrations and defects in ferromagnetic structures such as pipes [16–19]. The metal magnetic memory method is mainly applicable to soft ferromagnetic materials such as medium carbon steel commonly used in engineering. The basic principle is that a ferromagnetic material exhibits a force-magnetic coupling effect in which mechanical energy and magnetic energy are mutually converted as shown in Fig. 2 [20]. The basic theory of ferromagnetism suggests that the length of ferromagnetic materials placed in an external magnetic field changes due to variations in its magnetization state, as shown in Fig. 2a. That is, ferromagnetic materials have magnetostrictive property, which is also known as the Joule effect [21]. As shown in Fig. 2b, the applied stress changes the orientations of the magnetic domains inside the ferromagnetic material, which alters its magnetic properties. Thus, ferromagnetic materials have an inverse magnetostrictive effect, also known as the Villari effect [22] or the magnetomechanical effect [12]. The magnetostrictive and inverse magnetostrictive effects reflect

**Fig. 2** Schematic diagram of force-magnetic coupling phenomenon for ferromagnetic materials **a** magnetostrictive effect; **b** inverse magnetostrictive effects [20], Copyright@2017, Xidian University

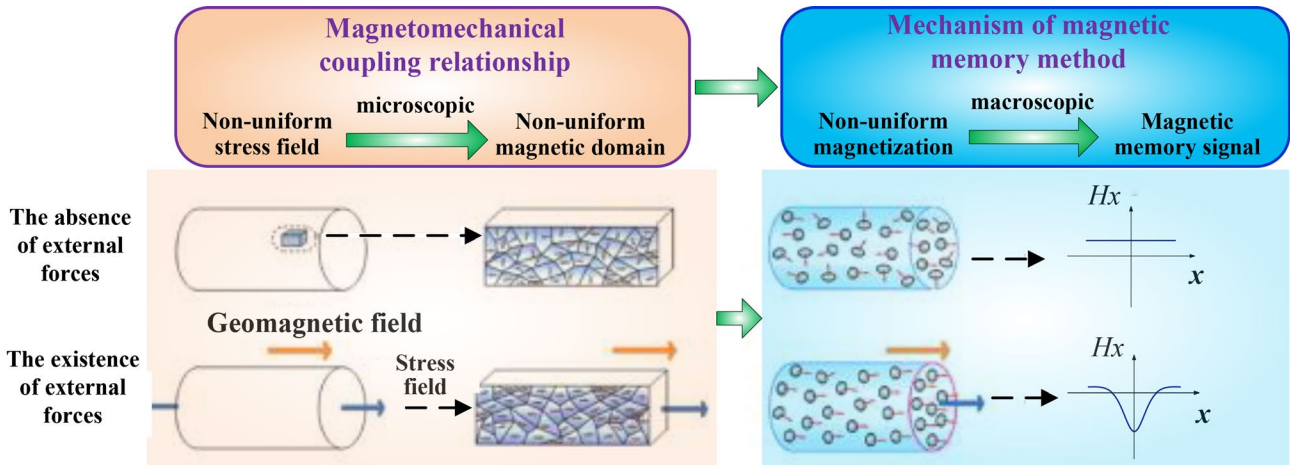
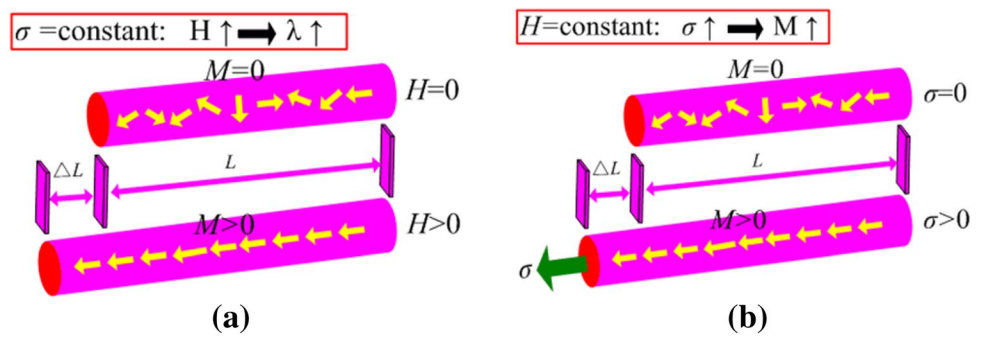


**Fig. 3** Schematic diagram of basic principle for the metal magnetic memory method [24], Copyright@2013, Acta Phys Sin

a mutual conversion between the stress and magnetism in ferromagnetic materials [23].

The principle of the MMM method is shown schematically in Fig. 3 [24]. Based on the Villari effect [22] or the magnetostrictive effect [12], the MMM method can evaluate the residual stress state inside of the ferromagnetic specimen. When a ferromagnetic material in a geomagnetic environment is subjected to an external force, its magnetic properties change because of the magnetostrictive effect of the material. Any defect or stress concentration affects the magnetostrictive effect, which in turn generates an MMM signal measured near the surface. By measuring the MMM signal near the surface of the specimen, the location and degree of the stress concentration zone or defect can be determined, allowing early diagnosis of the ferromagnetic material and its structural damage [25].

In 1970, Craik and Wood [26] performed the experimental measurement of magneto-mechanical curves with varying applied stress under the constant weak magnetic fields (the magnetic fields were 26.4 A/m, 80 A/m, and 132 A/m) for the polycrystalline ferromagnetic materials. Figure 4 shows the experimental results of changes in the magnetization with the varying stress under a weak constant magnetic

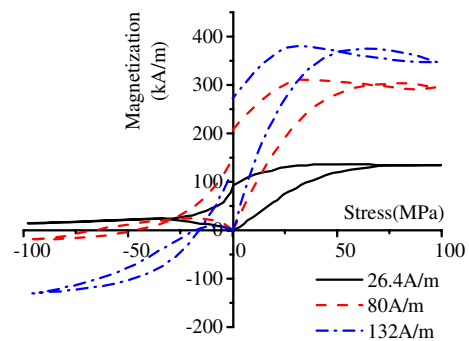


**Fig. 4** The experimental results of magnetostrictive effect under the constant weak external magnetic fields [26], Copyright@1970, Journal of Physics D: Applied Physics

field environment. It can be seen from the experimental results that: (i) with the increasing of stress, the magnetization increases at first, then drops, much slower for tension than for compression; (ii) on removing the tensile stress, the magnetization does not change along the original way, but increases at first and then drops; (iii) for the compression case, the magnetization always increases on the stress

removing and reaches its maximum value when the compressive is released opportunely. The experimental results prove that under a weak magnetic field environment such as the geomagnetic field, the change in stress causes change in the magnetization of the material. The magnetomechanical coupling effect is considered to be the basic principle of magnetic memory signal formation.

### 2.2 MMM Signal Characteristics

In Fig. 1, some non-linear characteristics of MMM signals near the stress concentration zone have been introduced. Researchers have been seeking various features of MMM signals to characterize the type and degree of damage.

Figure 5 shows schematics of the main feature quantities of MMM signals [20], and the characteristic parameters of the MMM signals that can reflect the stress concentration zone or damage mainly include the peak-valley interval and peak-valley value of the MMM signal component and its gradient.

Table 1 gives the relationship between each feature quantity and the defect size, lift-off value, and stress state [20]. Here, the three-dimensional volume defect with length, width and depth is discussed, and the lift-off value refers to the distance from the magnetic memory testing probe to the specimen surface. Researchers have proposed various characteristics to evaluate damage, stress, and defects of the materials. For example, Jian et al. [27] found that the gradient coefficient of the MMM signal can be used to judge

**Fig. 5** Schematic of characteristic parameters for MMM signals: **a** wave width  $\Delta x$  and peak-valley value  $\Delta H_x$  for tangential component; **b** peak-valley interval  $\Delta y$  and peak-valley value  $\Delta H_y$  for normal component; **c** peak-valley interval  $\Delta x$  and peak-valley value  $\Delta \text{Grad } H_x$  for gradient of tangential component; **d** wave width  $\Delta y$  and peak-valley value  $\Delta \text{Grad } H_y$  for gradient of normal component [20], Copyright@2017, Xidian University

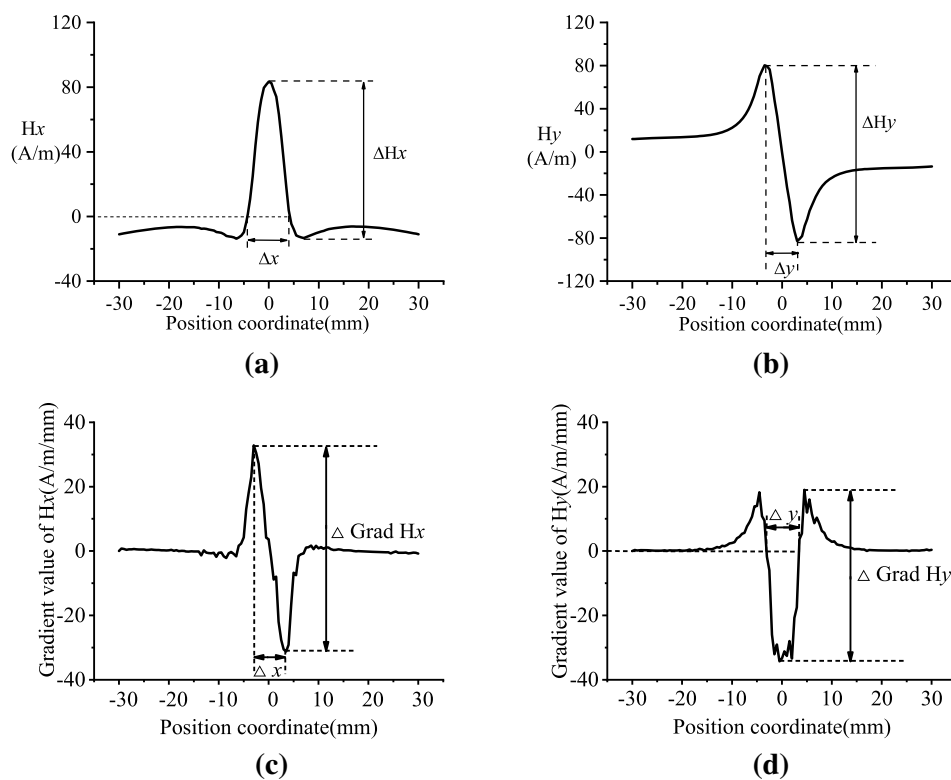


**Table 1** Correlation of MMM signal characteristics with defects and stress [20], Copyright@2017, Xidian University

Signal characteristics	Defect size			Other factors	
	Length	Width	Depth	Lift off	Stress
Peak-valley spacing of tangential components	+	~	+	+	+
Peak-valley difference of tangential components	+	+	+	-	+
Peak-valley spacing of normal components	+	+	+	+	+
Peak-valley difference of normal components	+	~	~	-	~
Peak-valley spacing of tangential gradient	+	~	~	~	~
Peak-valley difference of tangential gradient	+	+	+	-	+
Peak-valley spacing of normal gradient	+	-	+	+	+
Peak-valley difference of normal gradient	+	~	+	-	+

+, -, and ~ indicate positive correlation, negative correlation, and little influence, respectively

the critical state of materials. As shown in Fig. 6a, when a ferromagnetic material exhibits necking, the gradient of the MMM signal at the necking position appears nonlinear. Long et al. [28] showed the MMM method is effective for evaluating the effect of tempering and judging the degree of damage in each stage of the tempering process of tempered steel. Shui et al. [29] showed experimentally that the gradient of the MMM signal is effective for characterizing the stress-strain state of a ferromagnetic material during elastic deformation. Chen et al. [30] proposed a multi-lift method for accurate defects detection. To improve the reliability of the MMM method, Chen et al. [31] proposed the magnetic gradient tensor measurement and some analysis methods. Xu et al. [32] used the tangential component of the MMM signal to characterize the location and extent of buried cracks. Su et al. [33] proposed the difference of magnetic induction to reflect the fatigue state of the specimen by bending fatigue test of 45# steel as shown in Fig. 6b.

It should be noted that there are three magnetic vectors, magnetic field  $H$ , magnetization  $M$ , and magnetic induction  $B$ . There is some confusion in the literature over units. Confusion prevails because there are two ways that magnetostatics is presented. One is fictitious magnetic poles using the CGS (centimeter, gram, second) units, and the other is the current sources using the SI (International System) units. One can transform the physical quantity from one unit system into the other one according to the Table 2. Therefore, the magnetic induction strength in the air satisfies  $B = \mu_0 H$ ,  $\mu_0$  where is the magnetic permeability of air, and the value is often taken as vacuum permeability  $4\pi \times 10^{-7}$ .

### 3 Methods Proposal and Experimental Observations

#### 3.1 Methods Proposal and Validation

Doubov and colleagues examined the normal MMM signal measured near the surface of a ferromagnetic material under the combined action of tensile stress and magnetic field. The results showed that the position where the ferromagnetic material would eventually break was close to the zero point of the normal MMM signal, which meant that the characteristics of MMM signals could be used to determine the location of early damage in a ferromagnetic material. Based on this experimental phenomenon, Doubov and colleagues proposed the MMM method [10].

Immediately afterwards, Lin et al. [35] used the EMS-2000 intelligent MMM diagnostic equipment to detect welds in power-plant reheat pipes. By comparing the MMM results with those from ultrasonic testing, they confirmed that the MMM method could solve the problem of early damage diagnosis that conventional nondestructive testing methods could not. Huang et al. [36] compared the MMM method with the blind-hole method and acoustic emission technology. As shown in Fig. 7a, the test results showed that the magnetic induction intensity of the ferromagnetic material and the stress distribution therein varied in the same manner, thereby showing the feasibility of the MMM method for detecting the stress distribution in a weld zone. Zhang et al. [37] conducted preliminary

**Fig. 6** Change of magnetic induction intensity with number of cycle in the bending fatigue: **a** magnetic gradient under different applied force [27] Copyright@ 2009 Journal of Magnetism and Magnetic Materials; **b** difference of magnetic induction under different numbers of cycles [33]. Copyright@ 2016 Int J Appl Electromagn Mech

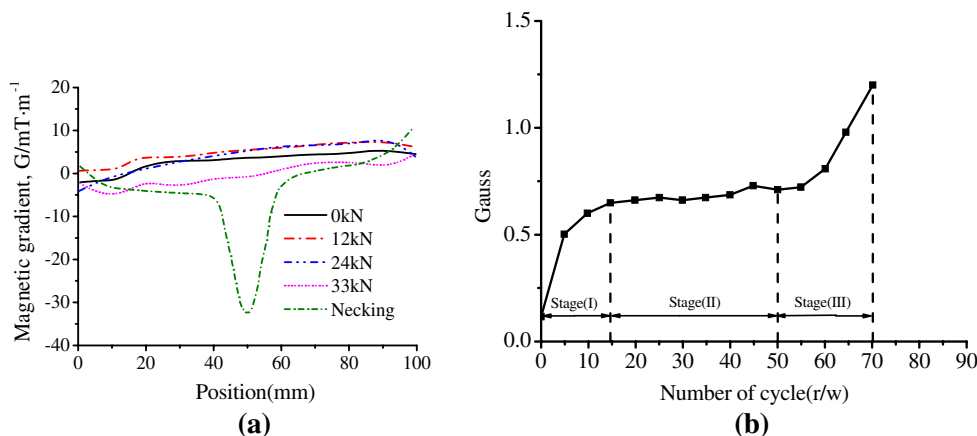
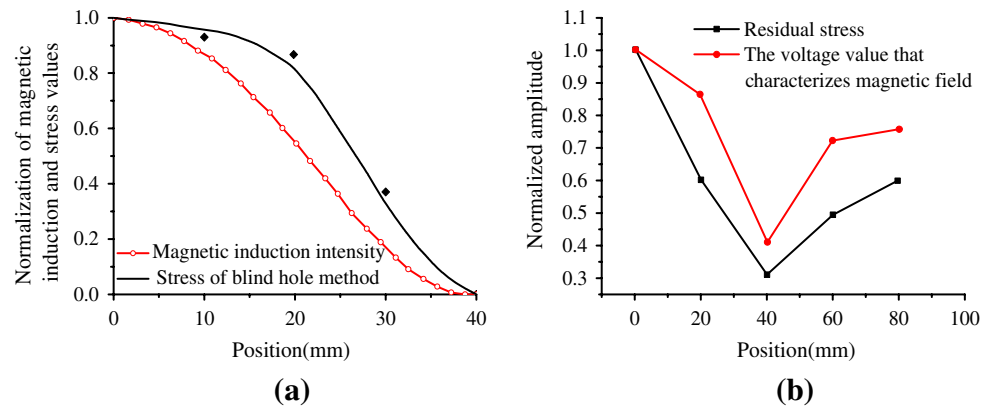


**Table 2** Conversions between CGS and SI units [34]

Magnetic term	Symbol	SI unit	CGS unit	Conversion factor
Magnetic induction	B	Tesla (T)	Gauss (G)	1 T = 10 <sup>4</sup> G
Magnetic field	H	A/m	Oersted (Oe)	1 A/m = 4π/10 <sup>3</sup> Oe
Magnetization	M	A/m	emu/cm <sup>3</sup>	1 A/m = 10 <sup>-3</sup> emu/cm <sup>3</sup>

A Ampere, cm centimeter, emu electromagnetic unit, m meter

**Fig. 7** Correlation between stress and magnetic induction in a ferromagnetic material: **a** normalized results for stress and magnetic induction [36] Copyright @ 2002 Nondestructive Testing; **b** relationship between residual stress and magnetic parameters [37]. Copyright @2005 Acta Armamentarii



discussions on the MMM phenomenon of high-strength steel such as gun steel and elastic steel, and their experimental results (see Fig. 7b) showed that the MMM method allowed the residual stress state to be analyzed quantitatively. Furthermore, Wilson et al. [38] confirmed the feasibility of evaluating the internal stress state of a material through the residual magnetic field measured near its surface in the absence of an external excitation magnetic field. Those early studies verified the feasibility of the MMM method and helped in its development.

Subsequently, researchers have tried to explain how the MMM signal is formed from macroscopic magnetomechanical effects and microscopic magnetic domains. Doubov [39] noted that when a ferromagnetic material is subjected to cyclic loading in a geomagnetic environment, the material generates a spontaneous magnetization and forms a

spontaneous MMM signal measured near its surface. Ren et al. [40] observed how the internal magnetic domains of alloy-20 stainless steel varied under stress, as shown in Fig. 8a. The results showed that the magnetic domains in a region of stress concentration in a ferromagnetic specimen change under the action of stress. When the stress is not concentrated or the stress concentration is small, the magnetic domains in the grains are mainly sheet-like domains, and the domain walls in the same crystal grain are parallel to each other. As the degree of stress concentration increases, the length and spacing of the domain walls change and labyrinth domains appear. Furthermore, as the number of labyrinth domains increases, the magnetization at the position of stress concentration becomes large, and a spontaneous leakage magnetic field forms near the surface. Qiu et al. [41, 42] investigated the characterization of applied tensile stress

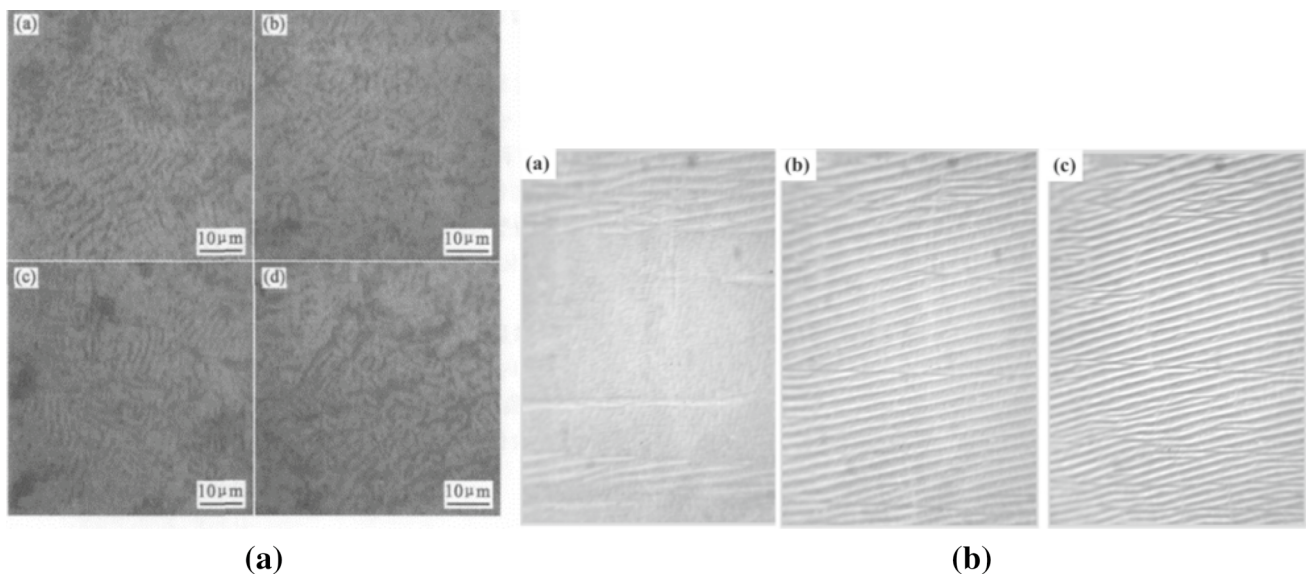


**Fig. 8** Variation of internal magnetic domains with loading stress: **a** different loads imposed on the magnetic domain structure of alloy-20 stainless steel [40]. Copyright @ 2008 Journal of Aeronautical Mate-

rials **b** magnetic domain patterns of HGO electrical steel under different loads [41] Copyright @ 2017 Journal of Magnetism and Magnetic Materials

with in-situ magnetic domain imaging and their dynamic behaviors by using magneto-optical Kerr effect microscopy. The experimental results show a good correlation between the microscopic magnetic domain structure and the applied tensile stress, as shown in Fig. 8b. These results indicate to some extent that the microscopic mechanism of MMM signal generation is the change of magnetic domains inside the material caused by the magnetomechanical effect.

### 3.2 Basic Morphology of MMM Signals

The mentioned researches show that the MMM method is effective for detecting stress concentration and early damage in ferromagnetic materials. Since then, there have been many experimental observations of MMM signals from non-defective and defective ferromagnetic materials under different working conditions [43–47]. The basic characteristics of MMM signals under different working conditions are shown in Table 3. As shown in Table 3, the normal component of magnetic memory signals for non-defective specimens is always almost linear change, and the tangential component is closer to a constant function under the action of elastic load [43]. When local plastic deformation of the material occurs, non-linear abrupt changes occur in the magnetic memory signals near the location of the plastic zone [44]. For ferromagnetic materials with defects, the normal component of magnetic memory signals exhibits a non-linear change near the defect, with maximum and minimum values appearing at the edge of the defect, and the absolute value of the tangential component reaches the minimum value near the defect location [45]. Compared with the circular hole defect, the non-linear change of the magnetic memory signal at the crack position is more obvious [46], and the signal change of the small defect such as the notch is the most obvious [47].

### 3.3 Experimental Observations of MMM Method

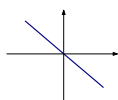
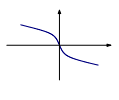
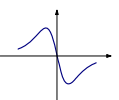
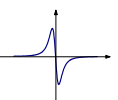
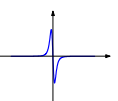
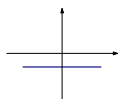
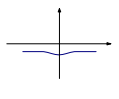
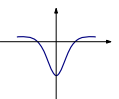
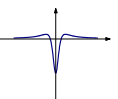
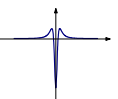
#### 3.3.1 MMM Signals of Non-defective Materials

Many researchers have studied how MMM signals from non-defective ferromagnetic materials vary under the combined effects of stress and magnetic field [48–53]. Figure 9 shows measured MMM signals from non-defective plate specimens under static loading with different stress levels [43], where Fig. 9a shows the normal component of the MMM signal and Fig. 9b shows the tangential component. The normal MMM signal from a non-defective test piece is always almost linear, the tangential MMM signal is close to a flat line, and (i) the slope and absolute values of the normal component and (ii) the tangential component of the MMM signal all increase with stress.

Figure 10 shows experimental results for non-defective specimens of different materials under static loading conditions [54]. For different ferromagnetic materials, how the MMM signal varies with stress remains essentially unchanged. For non-defective specimens of different ferromagnetic materials, the absolute value of the slope of the normal component of the MMM signal increases with stress. However, because the materials, dimensions, and experimental environments differ, so do the experimental values of the slope of the normal component of the MMM signal for different materials. Ren et al. [55] studied the magnetic induction intensity measured near the surface of no. 45 cold-rolled steel during stress loading and unloading.

There has also been much experimental research into how MMM signals change under other loads. Zhang et al. [56] studied how the MMM signals of the elastoplastic state of A3 steel varied under torsion. As shown in Fig. 11, the MMM signal at the center of the specimen remained basically constant with increasing torque, while those on either side had opposite trends with increasing torque. In addition, the signal strength of the elastic state of the test piece increased with torque, whereas that of the plastic state decreased. Xing et al. [57] studied how the MMM

**Table 3** Basic morphology of MMM signals

	Non-defective materials		Defective materials		
	Elastic [43]	Plastic [44]	Hole [45]	Crack [46]	Notch [47]
Normal signal					
Tangential signal					

Copyright © 2015 Strain; 2014 Beijing Jiaotong University; 2008 NDT and E International; 2017 J Press Vess Technol; 2010 Chinese Journal of Mechanical Engineering

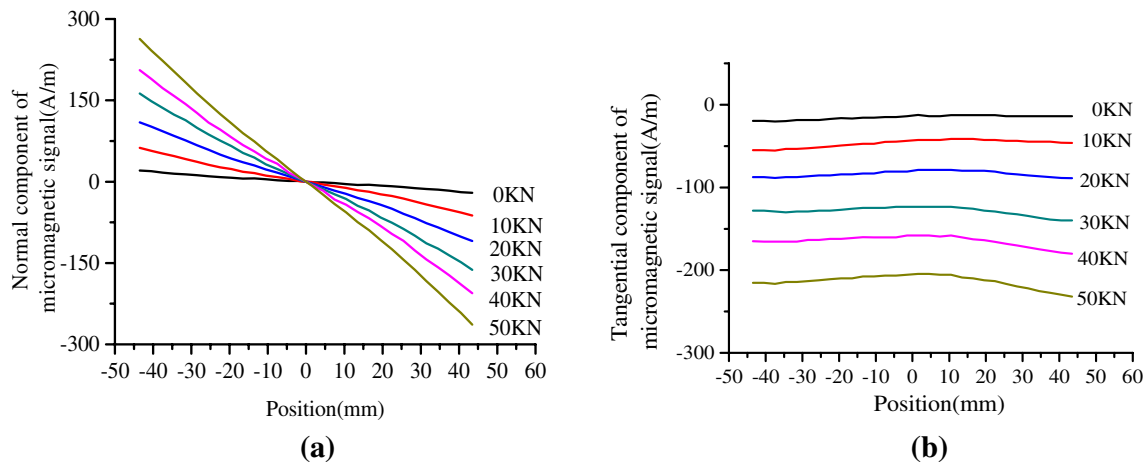


**Fig. 9** Surface MMM signal of non-defective U75V steel specimen [43]: **a** normal component; **b** tangential component. Copyright @ 2015 Strain

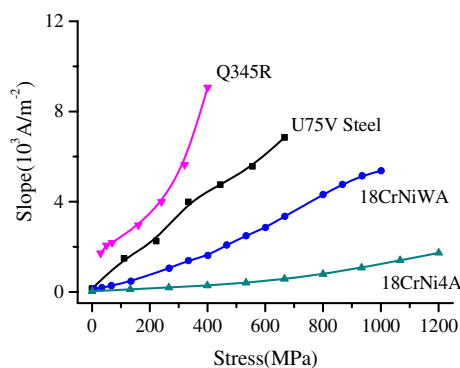


**Fig. 10** Characteristics of MMM signals of non-defective specimens of different materials [54]. Copyright@ 2017 International Journal of Mechanical Sciences

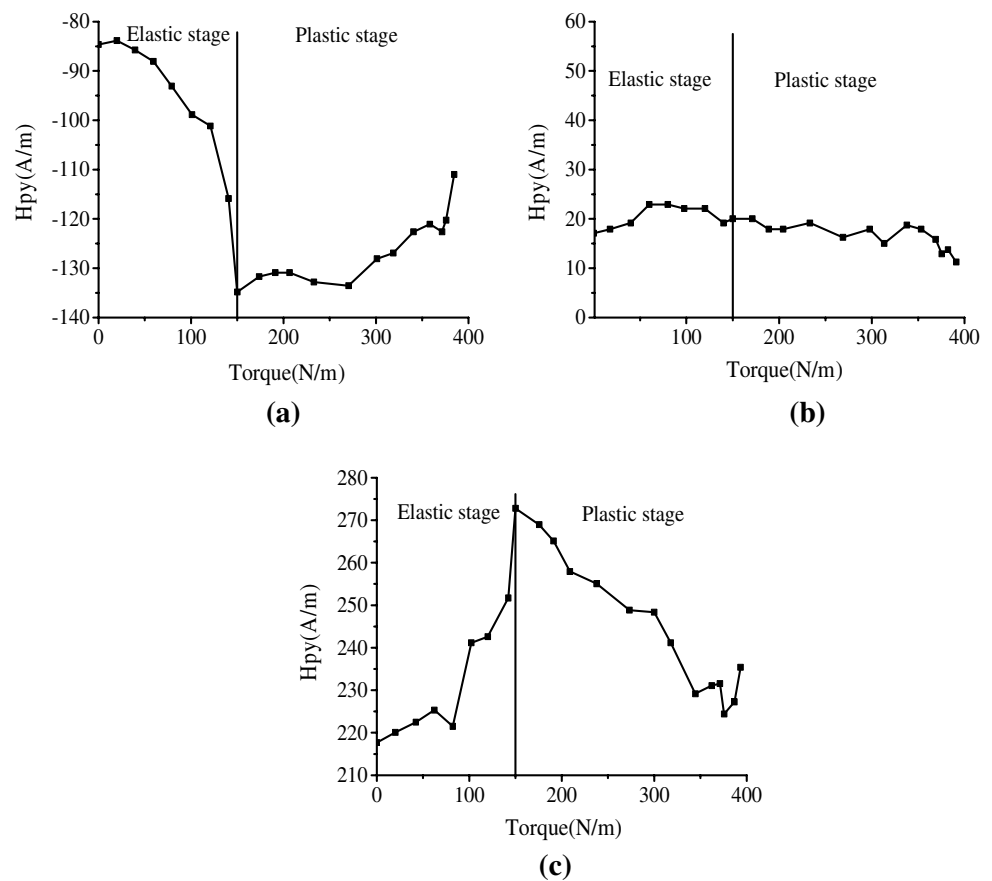
signal from Q235B varied under three-point bending and complex stress. The results showed that the MMM signals of the tensile and compressive layers of a ferromagnetic material are opposite and that the MMM signal is effective for evaluating the three-point bending deformation state of the material. Roskosz et al. [58–60] studied the relationship between the MMM signal distribution and the stress distribution of ferromagnetic materials in static tensile tests. Comparing the distributions in Fig. 12 shows that the correlation between the gradient of the MMM signal and the stress is better than that between the surface MMM signal and the stress. Hu and Yu [61] analyzed the variations in magnetic induction intensity with the surface residual compressive stress of 304 stainless steel specimens. Yao et al. [62] measured the relationship between the contact damage of no. 45 steel and its surface MMM signal under the action of ferromagnetic and nonferromagnetic indenters. And they proposed that the gradient

eigenvalue of the MMM signal can be used as a parameter for early contact-damage evaluation.

In addition, some studies have been conducted on how the MMM signal from a ferromagnetic material varies under plastic deformation. Li et al. [63] studied how the MMM signals of non-defective 1045 and A3 steel specimens varied under different plastic deformations; the results in Fig. 13 show that the slope of the normal component of the MMM signal decreased gradually with increasing plastic deformation. Li et al. [64] studied the MMM signal from AISI 1045 steel under tensile load and analyzed the loading influence on the MMM signal in the elastoplastic state through the magnetomechanical effect and the magnetoplastic model. Leng et al. [65] studied the MMM signals of Q235 steel under different deformation states; the results showed that the MMM signals differed greatly under elastic and plastic deformation and that small plastic deformation could decrease the MMM signal dramatically. Guo et al. [66] studied the MMM signal from 35CrMo steel under tensile load. The results showed that when the stress was less than the yield strength, the normal component of the MMM signal and its slope increased gradually with the stress, and when the stress approached the yield strength, the maximum value of the MMM signal was reached. Upon increasing the stress further, the normal component of the MMM signal and its slope both decreased drastically. Usarek et al. [67] also studied how plastic deformation affected the MMM signal. Qiu et al. [68] studied the MMM signal of Q235 steel entering yield failure from a lossless state; the results showed that the gradient of the normal component of the MMM signal could be used to determine whether the material had reached yield failure.



**Fig. 11** Variation of MMM signal with torque at different positions near the surface of Q235 steel [56] Copyright@ 2005 Journal of Beijing Institute of Technology



### 3.3.2 MMM Signals of Defective Materials

The basic characteristics of the MMM signals measured near the surfaces of defective ferromagnetic materials have also been observed, as shown in Fig. 14. The experimental results in Fig. 14b [69] show that the MMM signal on a defect-induced measurement line exhibits a typical nonlinear change: (i) the normal component of the MMM signal appears to increase first and then decrease; (ii) near the defect center, the tangential component of the MMM signal reaches its maximum value and the normal component crosses the zero point; (iii) the degree of the nonlinear change of the MMM signal increases with the size of the defect. Furthermore, the experimental results in Fig. 14c show how the peak-to-valley characteristics of the normal component of the MMM signal vary because of a defect; the experimental results show that the peak-to-valley values of the normal component of the MMM signal increase with stress [70]. Yao et al. [71] studied how the MMM signal measured near the surface of Q235 steel specimens with circular hole defects varies under compressive stress; the results show that the slope of the normal component of the MMM signal increases with the compressive stress, and the MMM signal exhibits nonlinear behavior near the defect. In addition, Bao et al. [43, 72] studied how the MMM signals

in U75V steel and Q345 steel with hole defects vary under static stress, and Li et al. [73] studied the MMM signals of Q235 steel with hole defects under tensile stress.

The above experiments all gave the distribution of the MMM signal on a certain measurement line but could not give the two-dimensional (2D) appearance of the MMM signal near a defect. Roskosz and Gawrilenko [45] measured experimentally the morphology of the MMM signal near a round hole defect in a plate, as shown in Fig. 15. The distribution of the MMM signal near the defect has the following characteristics: (i) the axial component of the MMM signal reaches its maximum value at the center of the defect, and there is a notched changing area either side of the defect; (ii) the tangential component of the MMM signal has four extreme points and  $180^\circ$  rotational symmetry; (iii) the tangential component of the MMM signal remains constant on the lines  $x=0$  or  $y=0$ ; (iv) the normal component of the MMM signal has two positive and negative extreme values, is symmetric about  $y=0$ , and the plus and minus extreme value reaches maximum on  $y=0$ ; (v) in addition, the position of the peak or valley extreme value of normal component coincides roughly with the edge of the round hole defect.

As well as the MMM signal induced by a circular hole defect as discussed above, researchers have also made

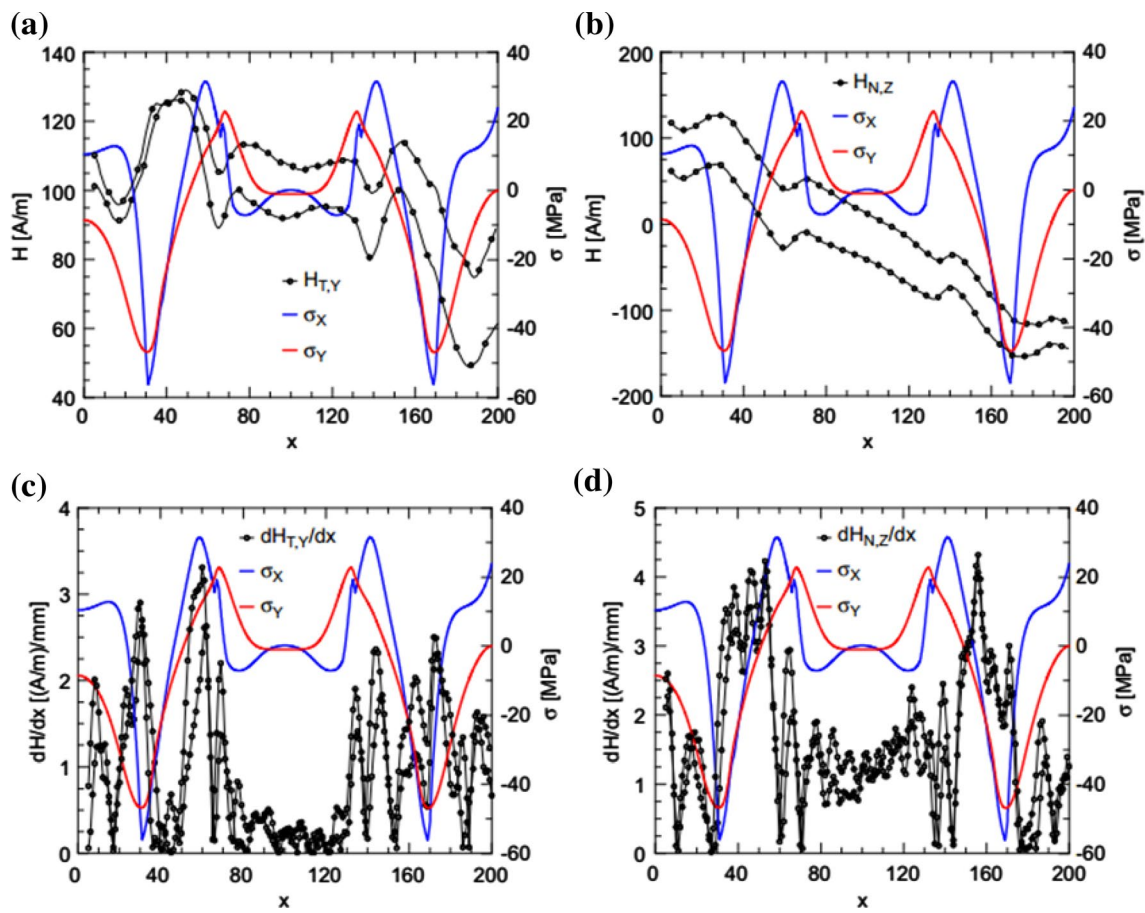
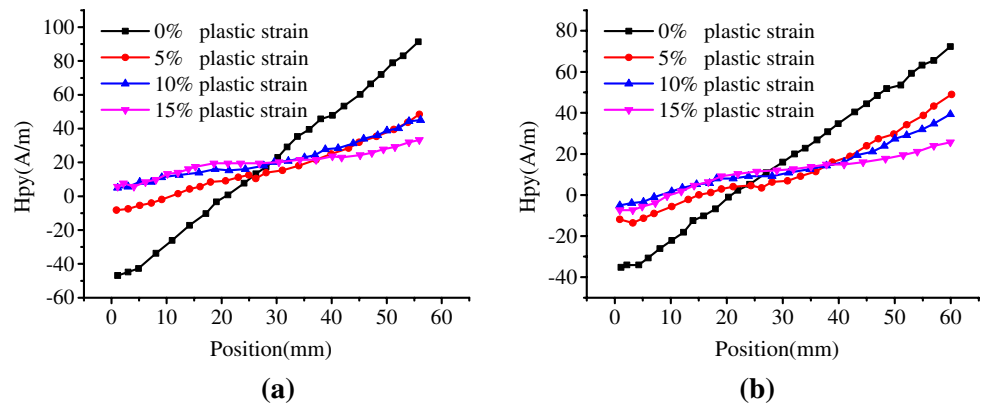


**Fig. 12** Comparison of MMM memory signal and stress distribution near the surface of Q345R steel: residual stresses  $\sigma_x$  and  $\sigma_y$  and a tangential component  $H_{T,Y}$ , b normal component  $H_{N,Z}$ , c tangential-

component gradient  $dH_{T,Y}/dx$ , and d normal-component gradient  $dH_{N,Z}/dx$  [58]. Copyright © 2012 NDT&E International

**Fig. 13** Variation of MMM signal with plastic deformation: a AISI 1045 steel; b A3 steel [63]. Copyright © 2012 Meccanica



experimental measurements of the MMM signals induced by secant, groove, and welding defects. Leng et al. [47] studied how the MMM signals induced by V-shaped defects varied under static tension and explained them through a magnetic-dipole theoretical model, as shown in Fig. 16a. Ren et al. [74] studied the variation of the

MMM signal induced by line cutting defects, as shown in Fig. 16b. Yu et al. [75] studied the variation of the MMM signal measured near the surface of an aluminum alloy sheet containing grooves. Li et al. [76] studied how the surface MMM signal from an alloy steel with groove defects varied under tensile stress and analyzed the

**Fig. 14** MMM signal measured near the surface of test piece containing defects: **a** sketch of specimen; **b** magnetic field distribution for specimens with holes of different radius  $a$  under a load of 14 kN; [69] Copyright @2013 Physics Examination and Testing; **c** peak-to-valley values of MMM magnetic field [70]; Copyright @2013 IEEE Trans Magn

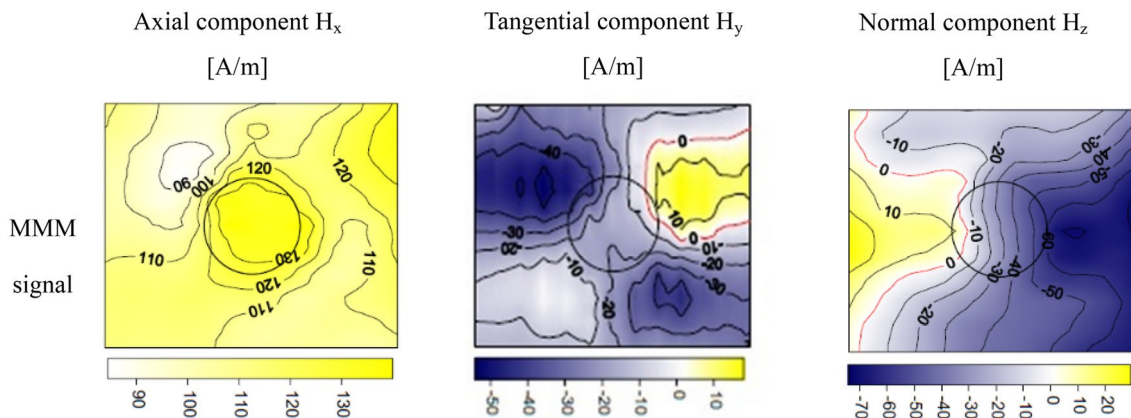
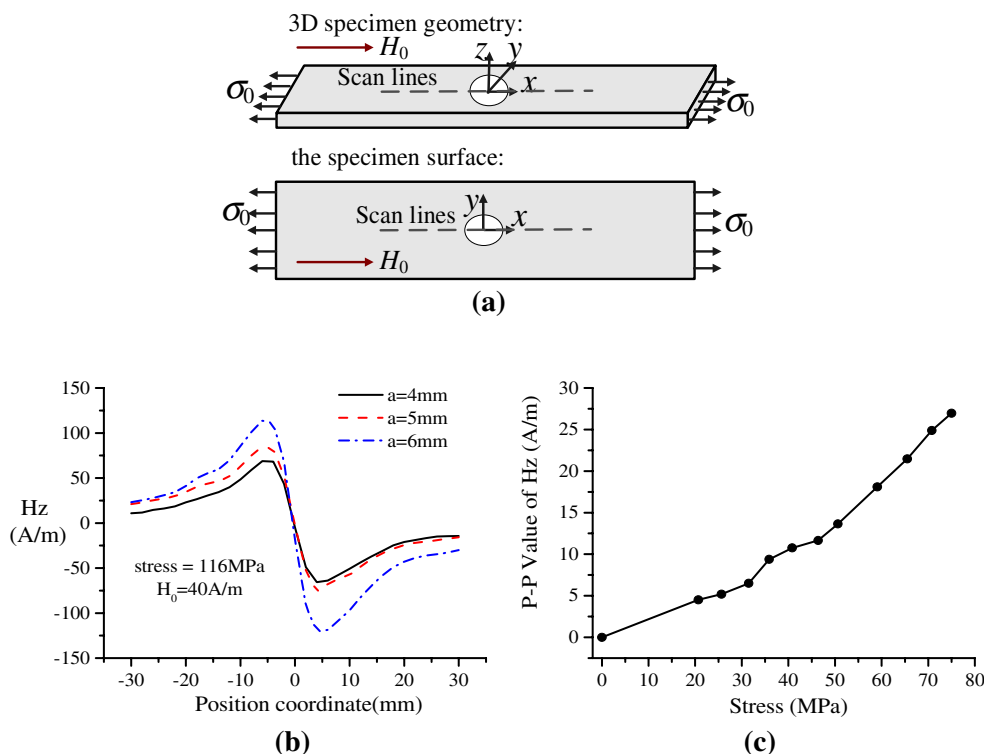


**Fig. 15** Morphologies of defect-induced MMM signal components [45]. Copyright @ 2008 NDT and E International

influence of multiple loading on the signal, as shown in Fig. 16c. Kolokolnikov et al. [77] studied the variation of MMM signals near welded joints in ferromagnetic materials. Li et al. [78] studied how the MMM signal from L80 steel with semi-cylindrical notches varied under static tension. Roskosz [79] studied the variation of the MMM signal at a weld in austenitic steel and concluded that defects could be detected accurately based on the MMM method in a service pipeline. Bao et al. [80] studied MMM signals measured near the surface of Q235 steel specimens with rectangular defects, analyzed the relationship between the signals and the degree of stress concentration, and studied

how the tangential component of the MMM signal changed with the stress state of the surface of a welding defect [81].

### 4 Qualitative Interpretation and Simulation

Through many MMM experiments, researchers have learned some basic rules regarding MMM signals and have tried to explain the underlying mechanisms. In this section, the existing work on the qualitative interpretation and simulation of MMM signals is summarized.

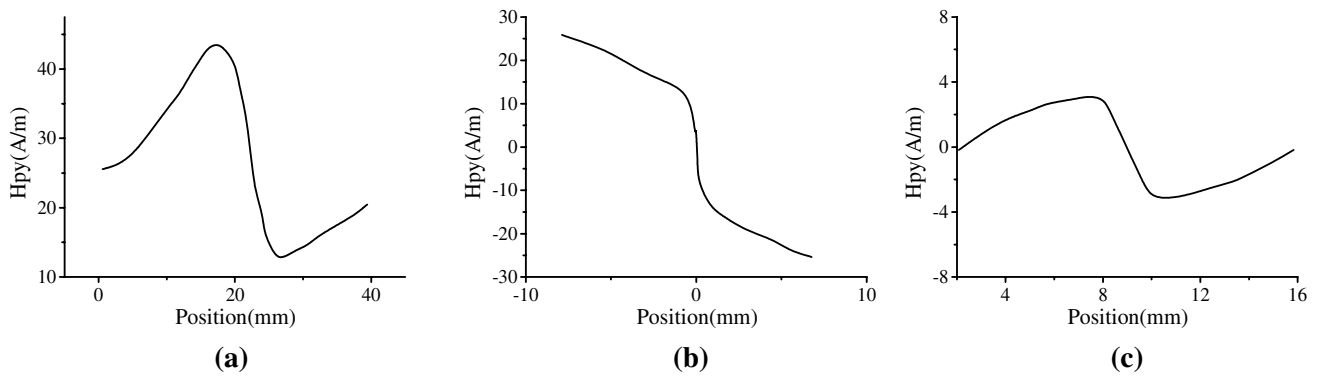


**Fig. 16** MMM signals induced by different types of defect: **a** Vshaped notch [47]; Copyright @ 2010 Chinese Journal of Mechanical Engineering; **b** secant [74]; Copyright @2005 Nondestructive Testing; **c** semi-cylindrical notch [76]; Copyright @ 2017 NDT&E International

### 4.1 Interpretation of MMM Signal Law

Some magnetomechanical models are commonly used to link mechanical and magnetic physical quantities. For example, based on magnetic-domain theory and magnetic-domain wall shift, the Jiles model [23], Zheng–Liu model [82] and Shi et al.’s model [83] are often used in the qualitative interpretation of MMM signals because of their clear physical mechanism.

#### 4.1.1 Inversion Phenomenon of MMM Signal

Yang et al. [84] used the expression for the effective field in the Jiles magnetomechanical model to explain the inversion phenomenon of the MMM signal from the defect surface as

the stress increases as shown in Fig. 17a. Based on the Jiles model, the effective field  $H_{eff}$  can be described as [23]

$$H_{eff} = H + \alpha M + \frac{3}{2} \frac{\sigma}{\mu_0} \left( \frac{d\lambda}{dM} \right)_{\sigma} (\cos^2 \theta - \nu \sin^2 \theta) \tag{1}$$

where  $H$  is the magnetic field,  $M$  is the magnetization,  $\alpha$  is the strength of the coupling of the individual magnetic moments to the magnetization  $M$ ,  $\sigma$  is the applied stress,  $\mu_0$  is the vacuum permeability,  $\lambda$  is the bulk magnetostriction,  $\theta$  is the angle between the axis of the applied stress and the axis of the magnetic field, and  $\nu$  is Poisson’s ratio. An empirical model can be used to describe the bulk magnetostriction [23], namely

$$\lambda = (\gamma_1(0) + \gamma_1'(0)\sigma)M^2 + (\gamma_2(0) + \gamma_2'(0)\sigma)M^4 \tag{2}$$

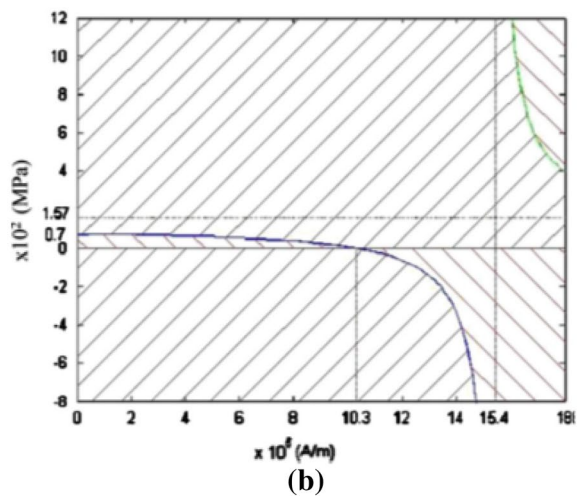
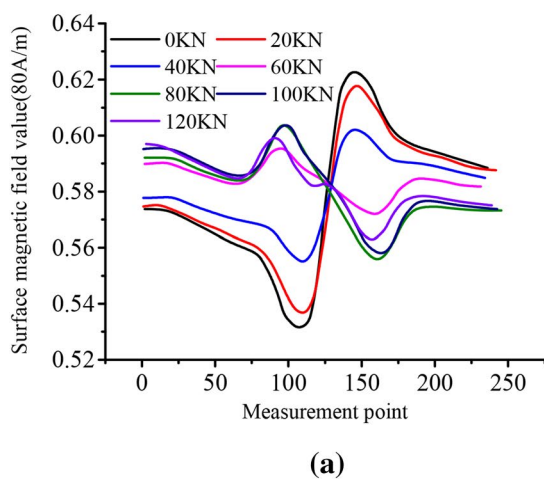


**Fig. 17** Variation of MMM signal measured near surface of ferromagnetic material with load: **a** variation of surface magnetic field by application of tension force under geomagnetic field; **b** anhysteretic magnetization varies along change of stress and initial magnetization,

where abscissa presents initial magnetization, ordinate presents stress [84]. Copyright @ 2007 Journal of Magnetism and Magnetic Materials

where  $\gamma_i$  are coefficients related to the material. In their experiment,  $\theta=26.5^\circ$  [84]. Then, using the magnetostriction data, the additional effective field can be given.

By studying the physical meaning of the above equation, Fig. 17b was plotted by giving the relationship among initial magnetization, stress, and resultant magnetization [84]. The above formula shows that when the initial magnetization is lower than  $1.54 \times 10^6$  A/m, applying a tensile stress of 70 MPa or more and applying all the compressive stress can decrease the magnetization. Only a tensile stress of less than 70 MPa leads to an increase in the magnetization. This is consistent with the experimental results.

### 4.1.2 Influence of Initial Magnetization State

Guo et al. [85] analyzed how the initial magnetization affects MMM signals by comparing the effects of initial magnetization and stress magnetization. As shown in the two sets of experimental results in Fig. 18a, b, stress influences the magnetic signal differently depending on the initial magnetization. In one experiment, the absolute value of the MMM signal first decreased and then increased with the stress. And MMM signal increases monotonically with increasing stress in another experiment. Guo et al. [85] explained this phenomenon as shown in Fig. 18c. Because the manner in which the surface magnetic field intensity changes is

consistent with the material magnetization, only the law for how the material magnetization changes needs to be analyzed. Here,  $M_i$  is the initial magnetization and  $M_\theta$  is the stress-induced magnetization. If  $M_i$  is as weak as the non-hysteretic magnetized  $M_{an}$ , then the former has little effect on the surface magnetization, and the surface magnetization increases with the stress. However, if  $M_i$  is strong and  $M_\theta$  is weaker than  $M_i$  because of low stress, then the surface magnetization decreases initially. As the difference due to  $M_\theta$  becomes smaller, the demagnetization state is reached when  $M_\theta$  is equal to  $M_i$ . Moreover, if the stress increases, then  $M_\theta$  predominates and the amount of surface magnetization reverses. Leng et al. [86] discussed how the initial magnetization influences the MMM signal by experimenting on 45# steel, and they explained the experimental phenomena qualitatively through the Jiles model. Ren et al. [87] measured surface MMM signals under static tension and explained the effects of different initial magnetization states using the magnetization model.

### 4.1.3 Local Equilibrium Under Cyclic Loading

Xu et al. [88] introduced the concept of local equilibrium to explain how the MMM signal from a ferromagnetic material varies with the number of stress cycles. By observing a rotating bending fatigue specimen, they found that the MMM

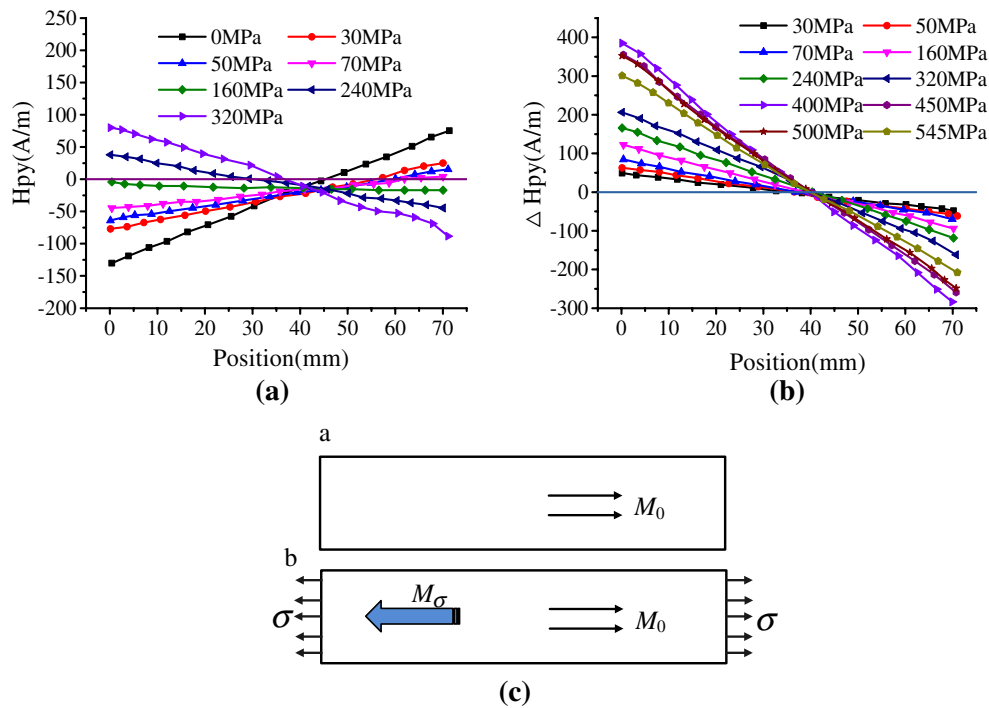


**Fig. 18** Effect of initial magnetization on MMM signals: **a** change of Hp(y) signals along testing lines; **b** change of Hp(y) signals along testing lines; **c** schematic of initial magnetization and its influence

on stress-induced magnetization [85]. Copyright © 2011 Journal of Magnetism and Magnetic Materials

signal in Fig. 19 gradually approached a local equilibrium state as the number of stress cycles increased. The MMM signal along the measurement line presented a stable loop within cyclic loading as shown. Xu et al. [88] explained this phenomenon by considering the local equilibrium state  $M_0$  based on the Jiles model. The relationship between the local equilibrium state  $M_0$  and the ideal magnetization state  $M_{an}$  is

$$(M_{an} - M_0)\mu_0 dH_{eff} = \delta k_1 dM_0, \tag{3}$$

where  $\delta$  is the symbol parameter and  $k_1$  is the pinning coefficient for the local equilibrium state  $M_0$ .

#### 4.1.4 Plastic Deformation Effects

Li et al. [89] made a plastic correction to the Jiles model so that as the plastic deformation increases, the MMM signal first decreases rapidly and then stabilizes, as shown in Fig. 20. They improved the expression of the effective field in the Jiles model to

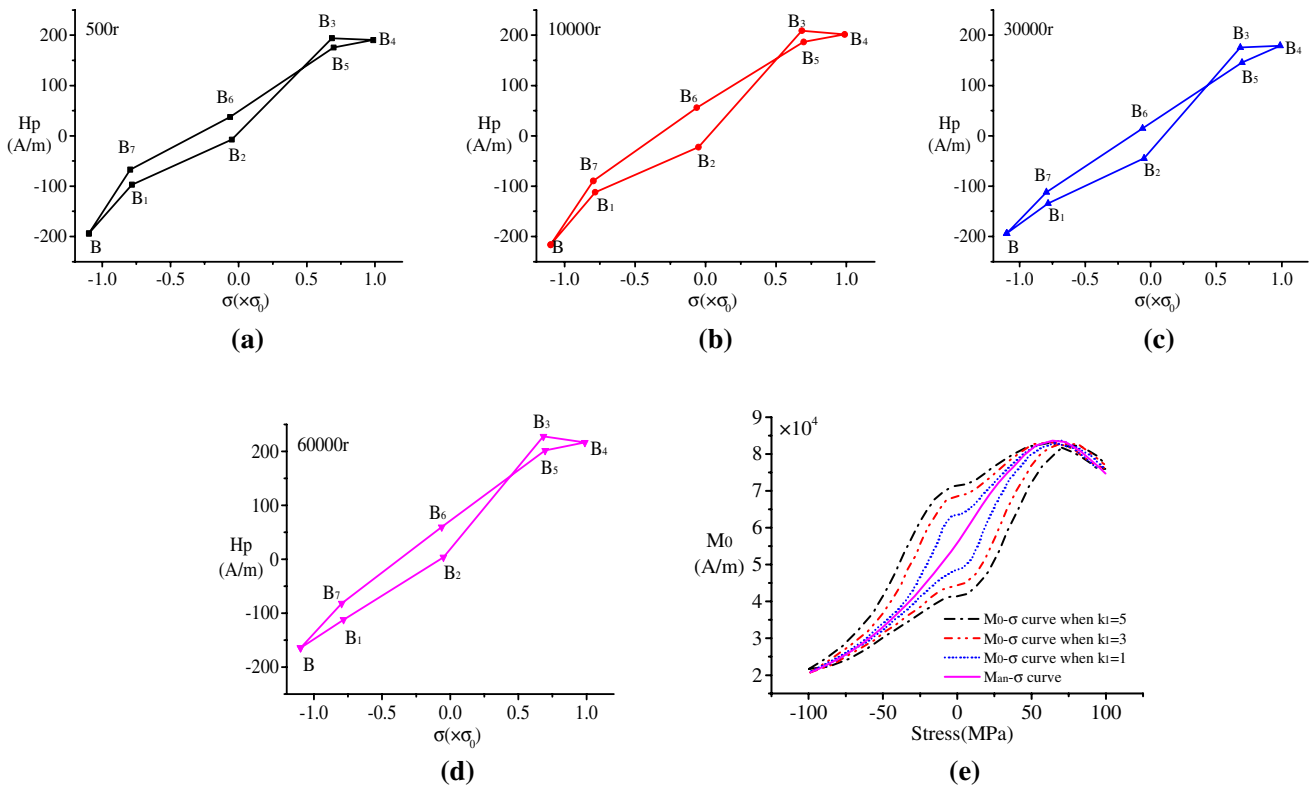
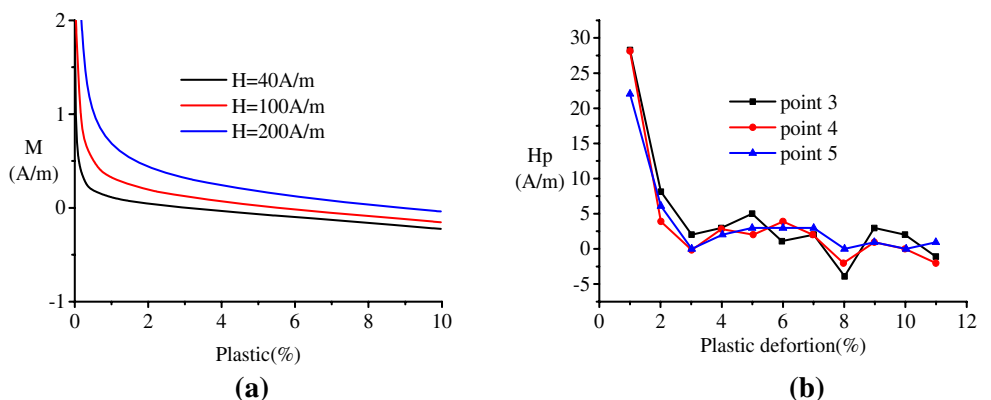


**Fig. 19** Variation of MMM signal with number of stress cycles: **a** 500 cycle; **b** 10,000 cycle; **c** 30,000 cycle; **d** 60,000 cycle; **e**  $M_0$ - $\sigma$  curves for different value of  $k_1$  when  $H = 40$  A/m [88]. Copyright @ 2012 Journal of Applied Physics

**Fig. 20** Variation of MMM signal with plastic deformation: **a** curves of magnetization vs. plastic strain under an applied magnetic field; **b** values of  $H_p$  vs. plastic strain measured at different points [89]. Copyright @ 2012 Journal of Applied Physics



$$H'_{eff} = H + \alpha'M + H_{\sigma r} + H_{\sigma p}, \tag{4}$$

$$H_{\sigma r} = \frac{3\sigma_r}{\mu_0} \frac{d\lambda}{dM}, \quad H_{\sigma p} = -\frac{1}{\mu_0} \frac{\partial E_p}{\partial M} = -k'|\epsilon_p| \tag{5}$$

where  $M$  is the magnetization;  $\sigma_r$  is the stress;  $\epsilon_p$  is the plastic deformation;  $\lambda$  represents magnetostriction;  $k'$  denotes the average density of pinning points per unit volume.

Leng et al. [90] used a similar approach to discuss how plastic deformation affects the MMM signal or magnetization effects. Yao et al. [91] showed how plastic deformation affects the magnetic properties of ferromagnetic materials through coercive force and magnetic permeability. Combined with ANSYS software, they analyzed how the size and location of the plastic zone, the lift-off value, and the detection direction influence the MMM signal. However, in the model of Li et al. [89] the magnetization is infinite at zero plastic strain and negative with increasing plastic strain; these features are obviously inconsistent with the common-sense view of how plasticity affects the magnetization. Shi et al. [92] further developed the magnetization model to achieve an accurate description of the effects of plastic deformation.

### 4.1.5 Effect of Stress on Magnetization

Roskosz et al. [58] used the Jiles model to explain some of the laws of MMM signals. Ren et al. [55] designed an MMM experiment to study the law governing stress magnetization during the loading and unloading of materials, and they used the Jiles model for experimental interpretation. Zeng et al. [93] used the magneto-optical method to observe and analyze the change of magnetic domain pattern of high permeability oriented electrical steel under different stress conditions. Results show that domain wall displacement is repeatable and stable both under cyclic stress round and during relaxation time after release of stress.

### 4.1.6 Magneto-elastoplastic Coupling Effect

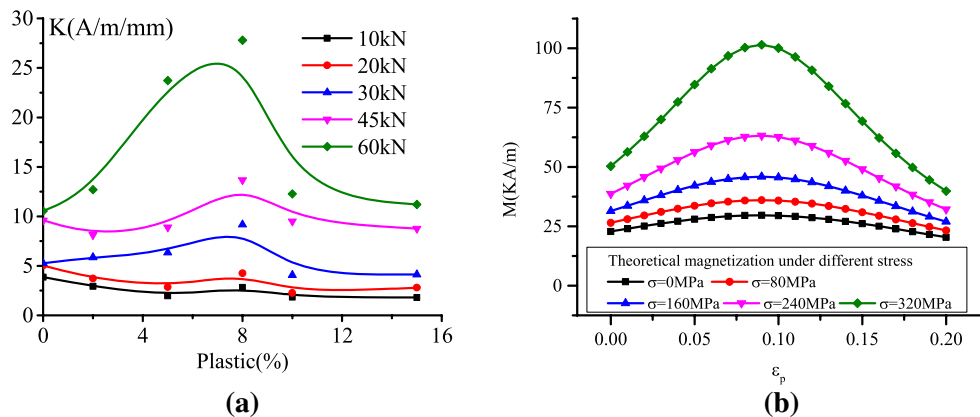
Shi et al. [94] introduced an experimental progress of the magneto- elastoplastic coupling phenomenon on MMM signal for ferromagnetic materials. The MMM signal was measured near the surface of medium carbon steel under the combined action of elastic load and plastic deformation. The experimental results show the magneto-elastoplastic coupling phenomenon as shown in Fig. 21a. The MMM signal increases with the increase of the elastic load, and the MMM signal increases first and then decreases with the increase of plastic deformation. As the elastic load increases, the effect of plastic deformation on the MMM signal gradually increases. They proposed an analytical theoretical expression of magnetization as [94]

$$M = \frac{H\mu_0 M_s^2}{3a\mu_0 M_s - 3\lambda_s(2kE\epsilon_p + \sigma_e) + (k'\epsilon_p^m - \alpha)\mu_0 M_s^2}, \tag{6}$$

where  $M$  is the magnetization;  $H$  is the environmental magnetic field;  $M_s$  is the saturation magnetization;  $\lambda_s$  is the saturation magnetostriction;  $m$  is used to describe the non-linear relationship between pinning density and plasticity;  $\sigma_e$  is the applied elastic stress;  $\epsilon_p$  is the plastic strain;  $E$  is the Young's modulus of the material;  $a$  and  $\alpha$  are a magnetization parameter;  $k$  is the conversion ratio of plastic strain energy;  $k'$  denotes the average density of pinning points per unit volume.

Equation 6 is an analytical theoretical expression of magnetization. When the magnitude of the external magnetic field and the elastoplastic conditions on the material are known, the theoretical value of the magnetization of the ferromagnetic material can be directly obtained through this expression. Figure 21b shows the theoretical result of the magnetization of the ferromagnetic material with the applied stress under constant plastic deformation. The variation of the magnetization with the elastoplastic state shown in Fig. 21b can well explain the magneto-elastoplastic coupling

**Fig. 21** Magneto-elastoplastic coupling effect **a** Experimental results of the slope variation of magnetic signal with stress and plastic deformation; **b** Model prediction of magnetization with stress and plastic deformation; [94] Copyright © 2020 Journal of Magnetism and Magnetic Materials



effect in the measurement result of MMM signal shown in Fig. 21a.

## 4.2 Simulation Work

Section 4.1 gives only a preliminary explanation of the experimental rules of MMM. Some researchers have also tried to simulate MMM signals using methods such as magnetic charge and magnetic dipole.

### 4.2.1 Magnetic Dipole Model

Based on the magnetic dipole model, Shi [95] obtained analytical expressions of MMM signals caused by four different surface defects, and discussed the effect of the complex shape of the defects on the strength and distribution of MMM signals near the surface. Huang et al. [96] studied MMM signals induced by cracks by referring to the processing method of magnetic flux leakage. Assuming a constant distribution of magnetic charge density measured near

the crack surface, the MMM signal was analyzed using the dipole method. Leng et al. [47] studied the characteristics of the MMM signal from a V-groove through experiments, as shown in Fig. 22; the results show that the MMM signal becomes nonlinear near the groove, and this nonlinearity increases with the load. Comparing the graphs in Fig. 22 shows that the simulation and the experiment give signals with similar morphologies. Recently, Shi et al. [94] present an analytical expression based the magnetic dipole theory to explain the abrupt phenomenon of MMM signal when ferromagnetic materials break.

### 4.2.2 Two-Dimensional Signal Simulation Based on Magnetic-Charge Model

By assuming a linearly distributed magnetic charge density in the surface stress concentration region of the material, Wang et al. [97, 98] used the dipole method to establish a theoretical model for the MMM signal near the stress concentration region. First, by the aforementioned assumption,

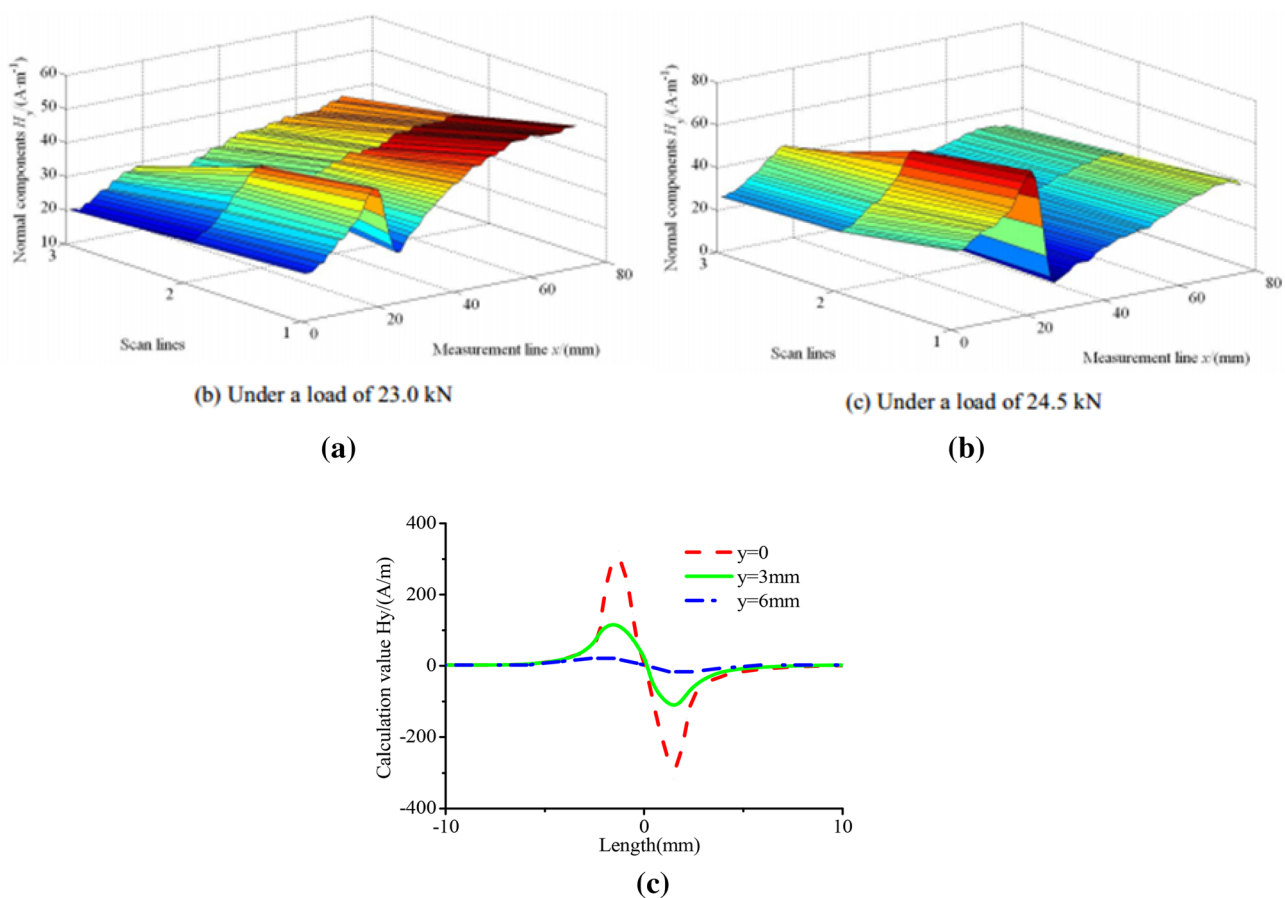


**Fig. 22** Characteristics of MMM signal induced by groove defects: **a, b** experimental values; **c** simulated values [47]. Copyright @ 2010 Chinese Journal of Mechanical Engineering



**Fig. 23** Schematic of magnetic-charge model in stress-concentration area: **a** one-dimensional (1D) stress-concentration area; [97] Copyright @ 2010 NDT&E International; **b** two-dimensional (2D) stress concentration area [98]. Copyright @ 2010 NDT&E International

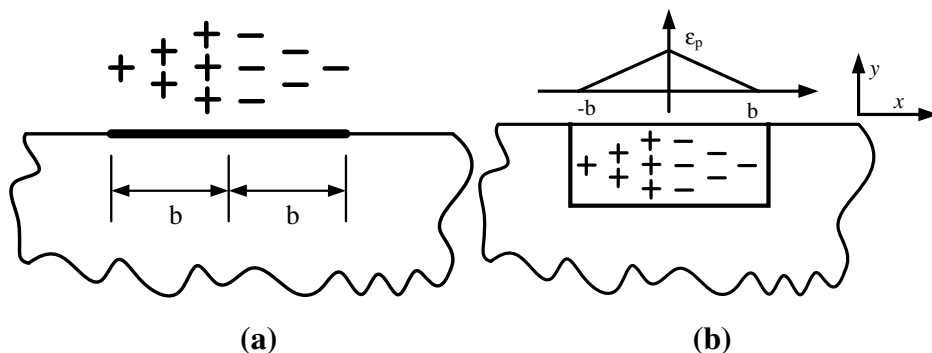
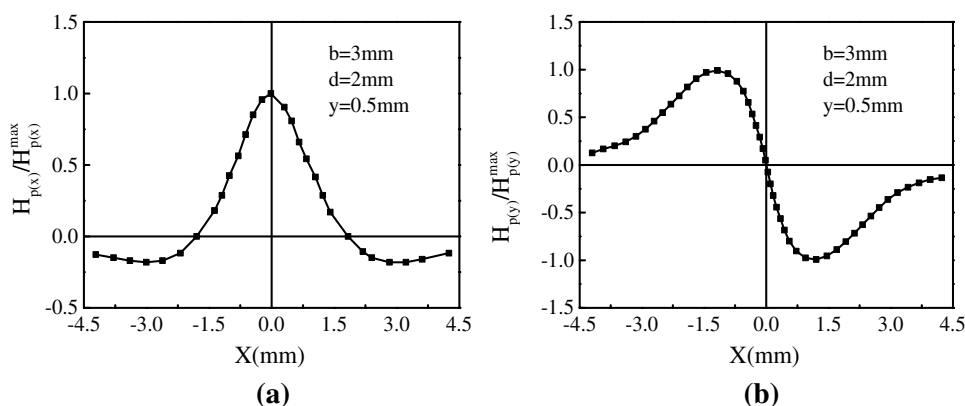


**Fig. 24** Simulation results for MMM signal based on model with 2D stress-concentration area: **a** tangential component; **b** normal component [98]. Copyright @ 2010 NDT&E International



they established a theoretical model of a one-dimensional (1D) stress concentration line using the dipole method. They also extended the 1D model to a 2D stress concentration model in further work, as shown in Fig. 23. Figure 24 shows the results of simulating the MMM signal in a 2D stress concentration zone [98]. The simulation results reflect qualitatively the nonlinear characteristics of the surface MMM signal near the stress concentration area. It is worth pointing out that there are some errors in the analytical expression of 1D stress concentration line [97]. Shi and Zheng [11] proposed a new analytical solution for the 1D stress concentration line problem, and confirmed the correctness of the new analytical solution by comparing it with the numerical solution.

### 4.2.3 Three-Dimensional Signal Simulation Based on Magnetic-Charge Model

In engineering practice, the actual geometry of the stress concentration zone usually has width. To cope with the shortcomings of the existing 2D stress concentration models, Shi and Zheng [11] proposed a three-dimensional (3D) stress concentration model of magnetic charge to advance and correct the previous 1D and 2D stress concentration models. As shown in Fig. 25, the plastic deformation is assumed to reach a maximum (resp. zero) on the axis of the stress

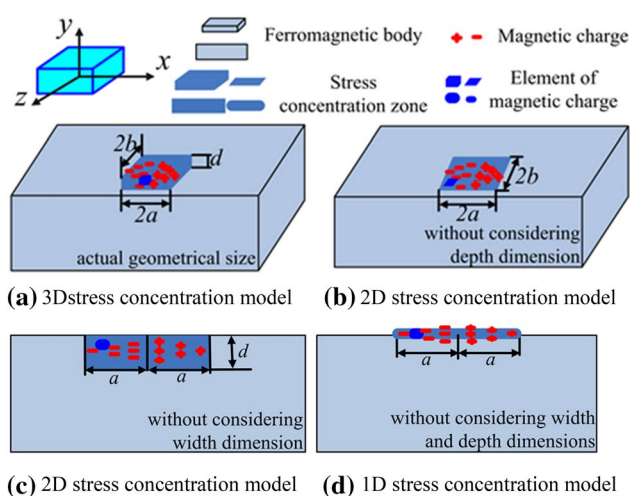


**Fig. 25** Schematics of magnetic-charge models for analyzing magnetic signals [11] Copyright@ 2016 Nondestructive Testing and Evaluation

concentration zone and decrease (resp. increase) linearly to zero (resp. maximum). By assuming a linear relationship between magnetic charge density and stress or plastic deformation, the 3D MMM  $H_m$  signal can be expressed as

$$H_m(\mathbf{r}) = \frac{\rho_1}{4\pi} \int_{-a}^0 \int_{-d}^0 \int_{-b}^b \left( \frac{m+a}{a} + \frac{\rho_0}{\rho_1} \right) \frac{\mathbf{r}}{|\mathbf{r}|^3} dmdndt + \frac{\rho_1}{4\pi} \int_0^a \int_{-d}^0 \int_{-b}^b \left( \frac{m-a}{a} - \frac{\rho_0}{\rho_1} \right) \frac{\mathbf{r}}{|\mathbf{r}|^3} dmdndt \tag{6}$$

where  $\rho = -\nabla \cdot \mathbf{M}$  and the magnetization  $\mathbf{M}$  under stress and magnetic field can be calculated by various magnetization constitutive relations.

As shown in Fig. 26a, the magnetic-charge model in the stress concentration area is compared with experimental

results [11]. The simulation results obtained using the magnetic-charge model are consistent with the experimental results, thereby confirming the effectiveness of the magnetic-charge model for simulating stress concentration and other damage. Figure 26b compares the new analytical solution [11], the previous analytical solution [97], and the results of numerical integration, indicating that there are problems with the analytical expressions in the existing literature [97].

Furthermore, theoretical results for the MMM signals measured near the surfaces of materials with long

**Fig. 26** Comparison of simulation and experimental results for MMM signal [11]. Copyright @2016 Nondestructive Testing and Evaluation

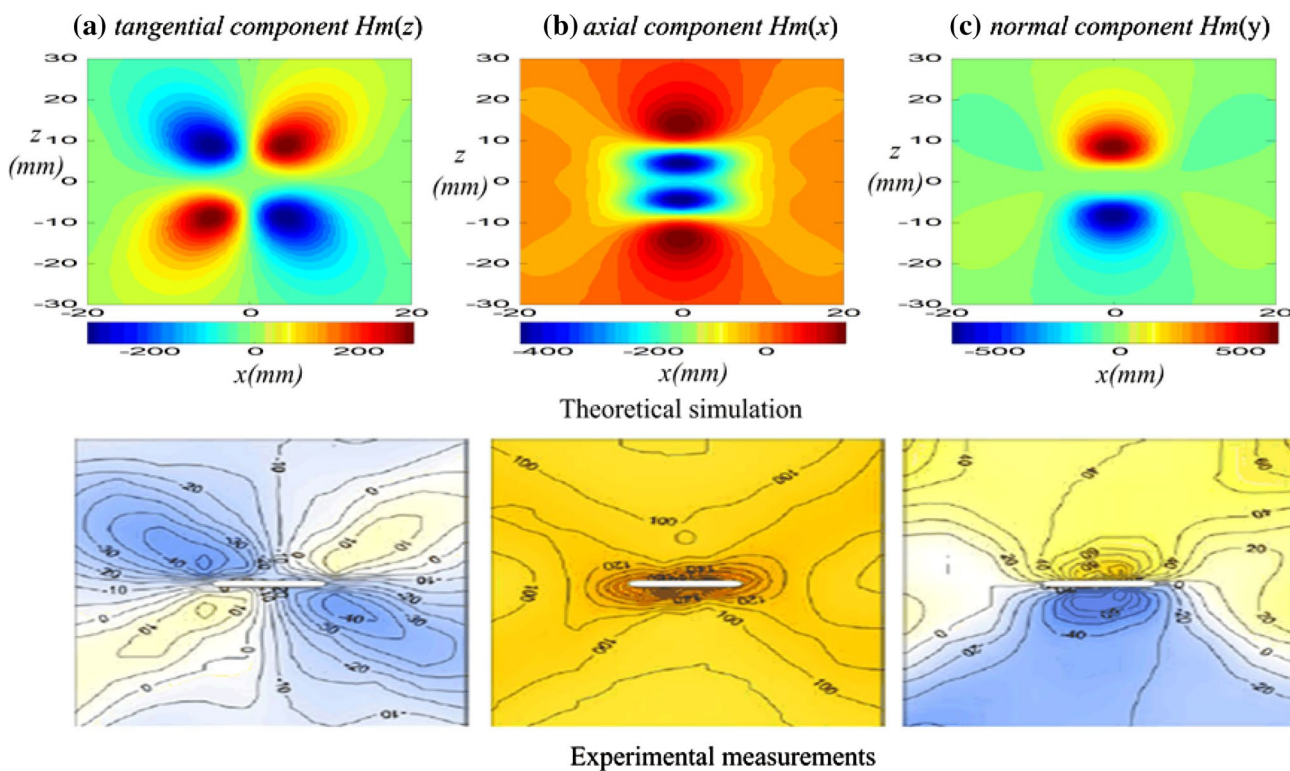
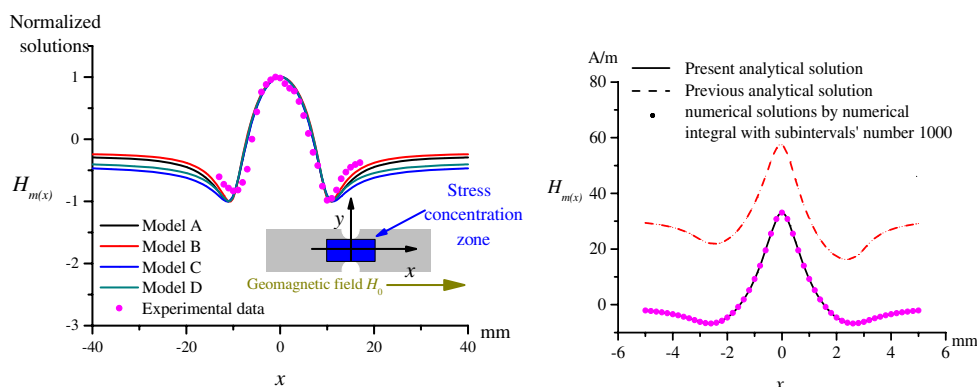


**Fig. 27** Distribution of crack-induced MMM signal; Simulation results; [11] Copyright @ 2016 Nondestructive Testing and Evaluation; Experimental results [99]. Copyright @ 2013 Meccanica

elliptical defects were obtained by using the magnetic-charge model. Figure 27 shows that the theoretical results for the MMM signal given by the magnetic-charge model agree well with the experimental results of Roskosz et al. [99]. Su et al. [100] used the magnetic-charge model proposed by Shi and Zheng [11] to reveal the effect of stress on MMM signals around defect by a tension tests of steel wire.

#### 4.2.4 First-Principles Method

Yang et al. [101] used a first-principles method to elaborate the mechanism for the magnetization of materials from a microscopic perspective. They used the first-principles plane-wave pseudopotential algorithm to establish the first-principles model. Then, by calculating the relationship among the lattice structure, atomic magnetic moment, and system energy and force, they studied how force influences the magnetic properties of materials and the relationship between atomic magnetic moment and pressure. Wang et al. [102] used the first-principles method to analyze theoretically the MMM signal from X52 pipe steel under stress. Liu et al. [103–106] studied the quantitative relationship between stress concentration and MMM signals by first-principles means and analyzed how material doping influences MMM signals. Figure 28 shows that the theoretical simulation results based on first principles reflect qualitatively the phenomenon whereby the MMM signal decreases with stress, but the theoretically predicted reduction of atomic magnetic moment is less than 1%, which is quite different from the experimental results. Therefore, this method requires further development to achieve a theoretical description of the law governing the MMM signal measured near the surface of a structure.

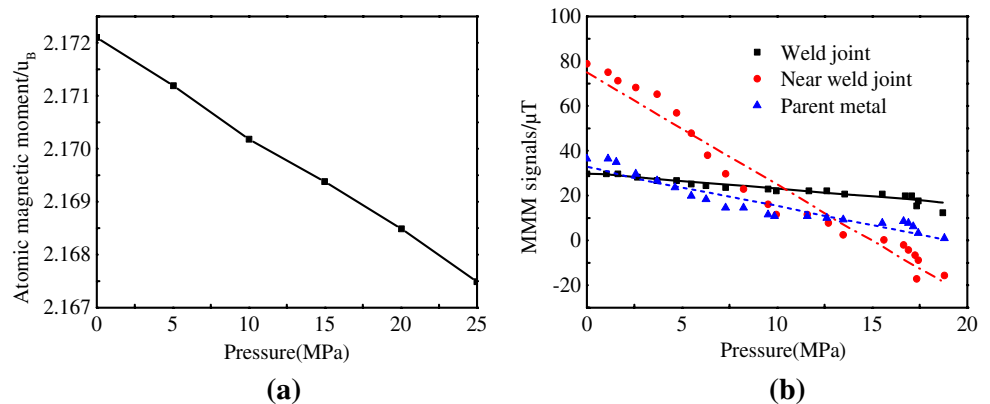
## 5 Quantitative Theory, Fatigue Process, and Natural Magnetization

### 5.1 Quantitative Theory

#### 5.1.1 Magnetostrictive and Inverse Magnetostrictive Effects

Because of the mutual transformation between stress and magnetism, the ferromagnetic materials have a typical non-linear magneto-elastic coupling effect including the magnetostrictive and inverse properties. Researchers have carried out a lot of theoretical researches on the magnetostrictive constitutive model for ferromagnetic materials, and the non-linear constitutive model based on thermodynamic model has been widely concerned. For instance, Carman et al. [107] proposed a standard square model based on the internal energy expansion and thermodynamic relationship of ferromagnetic materials. Wan et al. [108] proposed a hyperbolic tangent model by modifying the standard square model. Based on the assumption that the magnetostrictive strain is proportional to the square of the magnetization, a model is proposed by Duenas and Hsu [109]. In addition, Zheng and Liu [82] established a nonlinear constitutive model of ferromagnetic materials based on the macroscopic thermodynamic relationship and the microscopic physical mechanism. The Zheng-Liu model can accurately reflect the magnetic, magnetostrictive and elastic nonlinear characteristics of ferromagnetic materials, such as magnetization and magnetostriction saturation, and the prestress effects on magnetization and magnetostriction. Based on the Zheng-Liu model, subsequently, Zheng and her research team proposed a one-dimensional coupled hysteresis model of ferromagnetic materials considering temperature effects [110–112]. The one-dimensional coupled hysteresis model can well describe the effect of prestress on magnetization and magnetostriction of ferromagnetic materials at a given temperature. Jin et al. [113] established a magneto-thermo-elastic coupled

**Fig. 28** The phenomenon of MMM signal decreases with stress **a** Variation of atomic magnetic moment with pressure. **b** MMM signal distribution [104]. Copyright © 2015 Nondestructive Testing and Evaluation



hysteretic constitutive model of ferromagnetic materials by considering the reaction of the magnetization to magnetic field and the hysteresis effect. Further, Jin et al. [114] established a nonlinear structural dynamic model of ferromagnetic materials under dynamic magnetic field loading which can reflect the effect of excitation frequency.

The model mentioned above considers the magnetostrictive effect. Based on the Villaiy effect [22] or the magneto-mechanical effect [23], the MMM method can evaluate the residual stress state inside of the ferromagnetic specimen. As early as 1900, Ewing, a professor of Cambridge University, have published the monograph "Magnetic induction in iron, and other metals", which also included experimental results of magnetomechanical behavior of ferromagnetic materials in a constant magnetic field [115]. The study of magnetomechanical behavior under a constant weak environmental magnetic field plays an important role in quantitatively revealing the correspondence between MMM signals and damage in MMM method. To establish the relationship among stress, defects, and MMM signals more effectively, researchers have conducted forward modeling of MMM methods based on magnetomechanical relationships. Using the principle of energy conservation, a theoretical magnetomechanical formula for ferromagnetic materials was obtained [116]. Based on either this formula or similar empirical formulae for permeability [116], researchers have simulated MMM signals measured near the surfaces of various types of defect [116–120]. Li and Xu [121] considered the asymmetry of magnetomechanical behavior under tensile and compressive loads and proposed a modified Jiles–Atherton–Sablik model. Li et al. [70] analyzed theoretically the MMM signals caused by circular hole defects based on the Jiles model and the finite element method; the theoretical results and experimental data were well matched. Based on the Jiles model, Wang et al. [122] and Yao et al. [123] enhanced the effective field with that due to plastic deformation, established

a magnetic–elastic–plastic coupling model, simulated the MMM signal using the remanence variation caused by plastic deformation, and studied the MMM signal generated by the plastic deformation of ferromagnetic material. Bai et al. [124] also explained the MMM signal using the concept of remanence based on the Jiles hysteresis model. Avakian et al. [125] extended the magnetomechanical coupling model to multiaxial loading and analyzed how the loading direction affects the magnetization of the material. Moonesan et al. [126] analyzed how the initial magnetization of the material influences the magnetic signal through the magnetomechanical coupling model.

### 5.1.2 Magnetomechanical Coupling Forward Model for MMM Method

In 2017, Shi et al. [54] established a nonlinear magneto-mechanical coupling forward model. The finite element method was used to achieve the forward analysis of the MMM method, which describes quantitatively how surface MMM signals vary because of stress concentration and defects. Table 4 compares the prediction of MMM signals for several existing classical forward models. Comparing with the experimental data for the non-defective U75V test specimens of Bao et al. [43], it is found that the new magnetomechanical forward model established by Shi et al. [54] has an advantage in quantitative analysis of MMM signals. The theoretical model is good at predicting how the MMM signal varies with the stress measured near the surface of a non-defective specimen during the elastic phase, as shown in Table 4. The theoretical results from the energy conservation model, the mean value of tangential component and the slope of normal component of magnetic memory signals do not vary with the stress. The theoretical results from residual magnetization model and Jiles magnetomechanical model can both reflect the variation trend of characteristic value

**Table 4** Abilities of several forward models to predict MMM signals for non-defective specimens (points: experiment; line: theoretical prediction) [54]. Copyright © 2017 International Journal of Mechanical Sciences

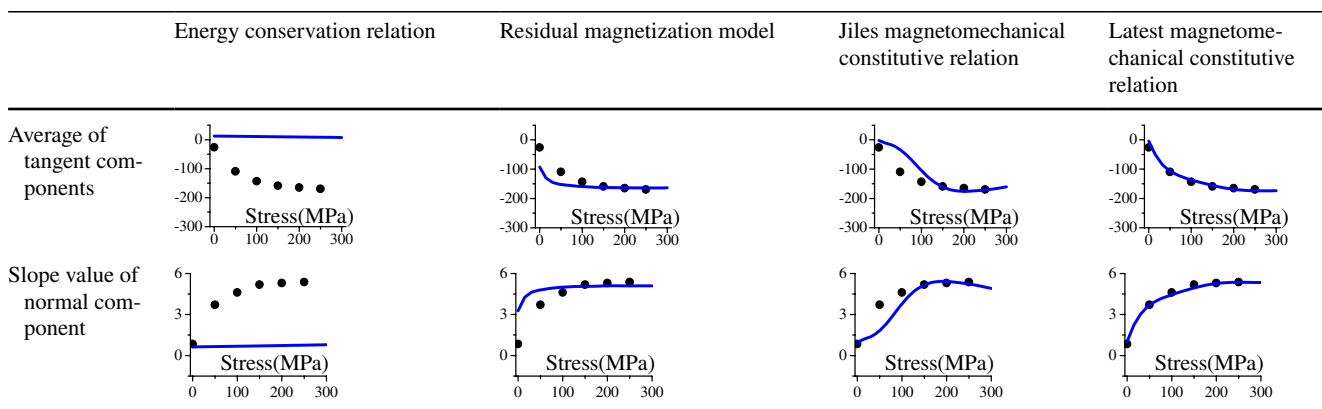


**Fig. 29** Comparison between predicted results and experimental data for MMM signals measured near surface of ferromagnetic material with circular hole defects: **a** MMM signals; **b** P-P value of MMM signals [54]. Copyright @ 2017 International Journal of Mechanical Sciences

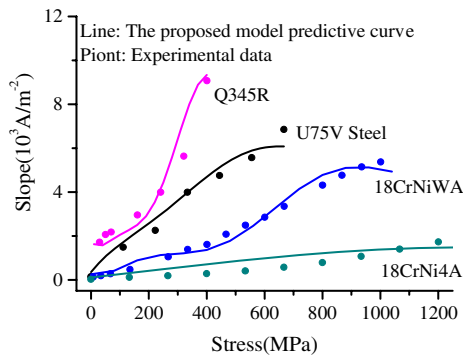
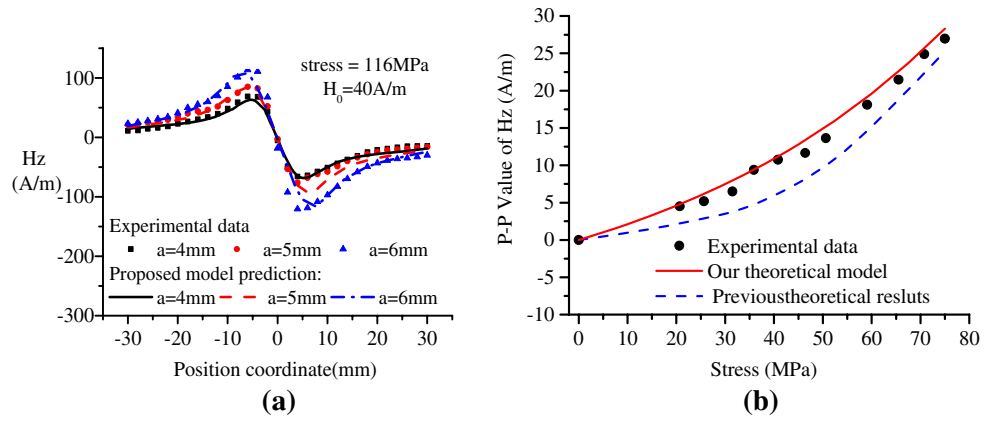


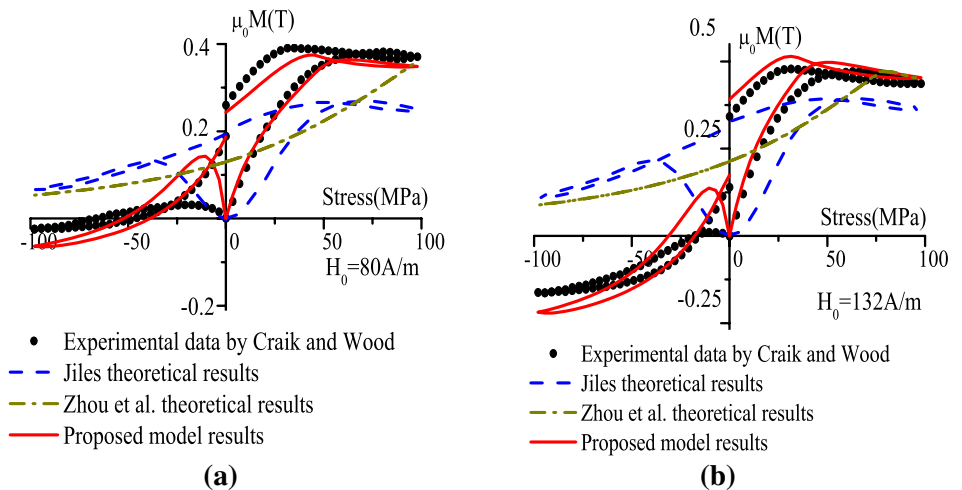
**Fig. 30** Comparison between theoretical and experimental values of MMM signals for various ferromagnetic materials [54]. Copyright @ 2017 International Journal of Mechanical Sciences

with the increasing stress, but there has a significant difference between the theoretical results and the experimental data for the low stress state. Compared with other classical models, the new calculated results agree quantitatively well with experimental data, and the MMM signals are described quantitatively well.

In addition, combining with the finite element method, the theoretical analysis of magnetic memory method can be obtained for ferromagnetic specimens with defects. The results from the proposed magnetomechanical model [54] were more coincident with the experimental data for different size of defects as shown in Fig. 29a. The validity of proposed magnetomechanical model to different load case was performed as shown in Fig. 29b. Comparison with the previous Jiles model shows that proposed magnetomechanical model is quite coincident with the experimental data for different stress states [54]. Figure 30 also showed the comparison of the theoretical prediction and the experimental results for slope change behavior of magnetic memory signal normal component for various ferromagnetic materials, which shows that the proposed magnetomechanical model is applicable for various ferromagnetic materials.

The new nonlinear forward model can reflect accurately how the MMM signals of ferromagnetic materials vary under various operating conditions. This is because the magnetomechanical constitutive relationship that the established reflects accurately how the magnetization of ferromagnetic materials varies under the combined action

**Fig. 31** Comparison between experimental data and magneto-mechanical curves predicted by magnetomechanical constitutive model **a**  $H_0=80$  A/m and **b**  $H_0=132$  A/m [83]. Copyright@2016 Journal of Applied Physics



of magnetic field and stress [83]. Starting from the Gibbs free energy of ferromagnetic materials and combined with the magnetization of ferromagnetic materials and Rayleigh's law, Shi et al. [83] proposed a magnetomechanical constitutive relation for weak magnetic fields. Comparing with the classic experiments by Craik and Wood [26] shows that the new constitutive relation agrees well with experiment and reflects accurately the magnetization behavior of ferromagnetic materials under compressive stress. Figure 31 compares the predictions of the new constitutive relation with Craik and Wood's experimental results [26] and with the predictions of other theoretical models. Compared with the Jiles constitutive relation, the theoretical results of the new constitutive relation are more consistent with the experimental results, especially under compressive stress. In addition, the new constitutive relationship reflects more accurately how the magnetization varies with stress in a weak magnetic field. In Fig. 32, the magnetomechanical curves of ferromagnetic materials under different initial magnetization states predicted by the newly constructed constitutive relation are compared with experimental data. It can be seen that this model reflects well how different initial magnetization states influence the magnetomechanical curve of ferromagnetic materials and agrees well with the experimental results.

Based on the magnetomechanical constitutive relation [83] and nonlinear forward model [54], Wu et al. [127] performed a theoretical analysis to perfectly explain the influence of stress distributions on 3D MMM signals for a wide plate tensile specimens without and with a defect. Shi et al. [92] further established a magnetomechanical constitutive relation for ferromagnetic materials considering the effects of temperature, elastoplastic state, and a weak magnetic environment. Using this constitutive relation, they established a nonlinear thermal–magnetic–elastic–plastic coupling forward model for MMM detection. Comparison with experimental data confirmed that the theoretical model is

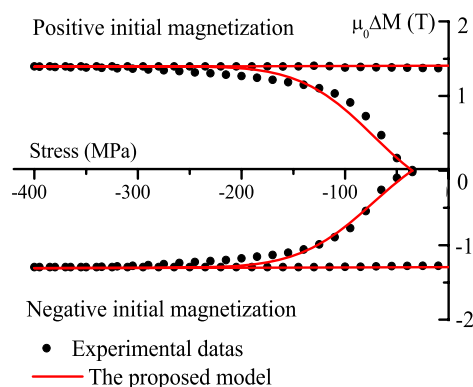


**Fig. 32** Comparison between theoretical prediction and experimental data for magnetomechanical behavior under different initial magnetizations [83]. Copyright © 2016 Journal of Applied Physics

accurate in describing how thermal–magnetic–elastic–plastic coupling factors influence the MMM signal in a complex environment. Recently, Zhang et al. [128] extended the magnetomechanical model to be applicable to magnetocrystalline anisotropy to study the angle effect on the MMM method.

## 5.2 Fatigue Process

The MMM method faces some new challenges in practical applications. For example, the components in actual situations are often subjected to long-term cyclic loading, and MMM signals often change with the number of cycles. This means that the selection of feature quantities for damage determination and the formulation of quantitative schemes must also consider the effect of the number of cycles. Therefore, it is necessary to study how MMM signals evolve under cyclic loading.

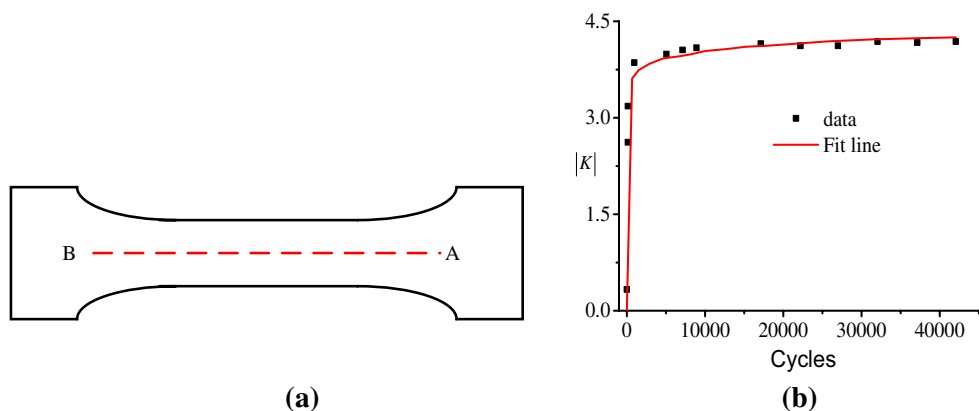
### 5.2.1 MMM Signals in Fatigue Tests of Non-defective Specimens

First, the results of measuring MMM signals in fatigue tests of non-defective specimens are introduced. Yuan et al. [129] conducted dynamic tensile tests on Q235 steel specimens and found that the number of cycles of elastic loading had no significant effect on the MMM signal; when the load amplitude was increased to produce plasticity, how the MMM signal varied with stress was opposite to that of elastic loading. Yan et al. [130] studied how the MMM signal from 20G pipe steel varied in a tensile fatigue test; the results showed that the MMM method was effective at determining the location of stress concentration in the material. Duan et al. [131] performed repeated loading–unloading tensile tests on round bar specimens made of 40Cr steel to determine the relationship between the MMM signal and tensile stress, and they found a magnetomechanical reversal when a specimen was subjected to a force that exceeded the yield strength. Shi et al. [132] studied the law governing the variation of the MMM signal from the surface of an 18CrNi4A specimen based on a tensile fatigue test, as shown in Fig. 33; for a non-defective test piece, the slope of the normal component of the MMM signal increased gradually with the number of loadings.

### 5.2.2 MMM Signals in Fatigue Tests of Defective Specimens

Here, the results of measuring MMM signals in fatigue experiments with defective specimens are introduced. Wang et al. [133] measured and analyzed how the MMM signal from no. 45 steel varied during the propagation of fatigue cracks. Wang et al. [134] investigated the mechanism for the generation and accumulation of MMM signals

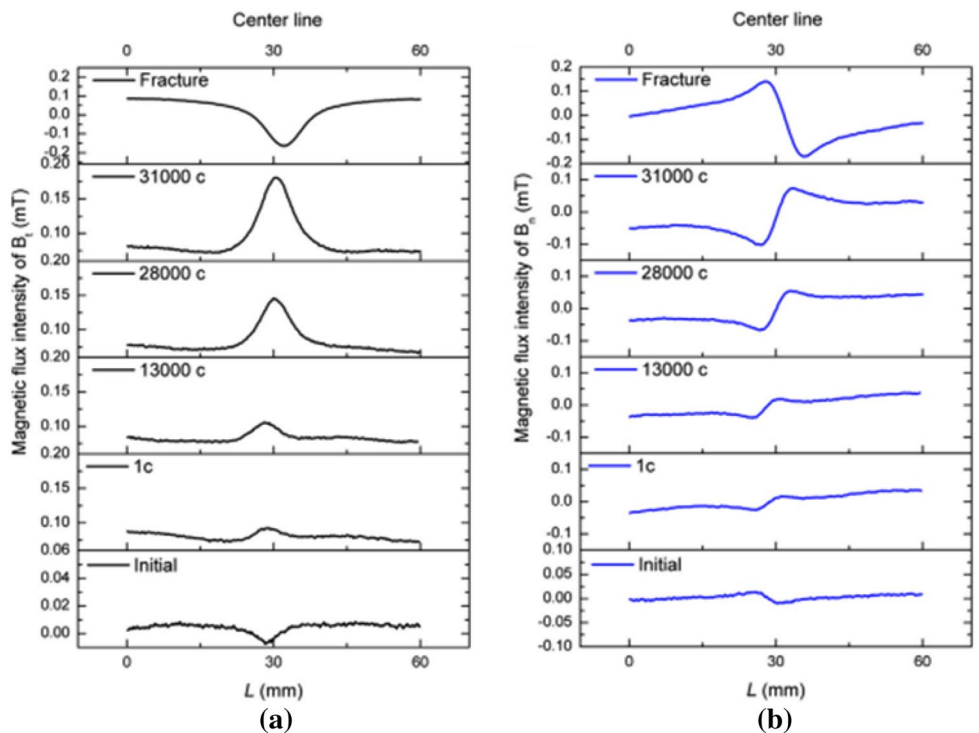
**Fig. 33** Change of MMM signal measured near surface of material with loading time: **a** specimen shape and measured path; **b** gradient  $k$  of magnetic signal at different cycles of specimen [132]. Copyright @ 2010 NDT & E International



based on cyclic-loading experiments on Q235 specimens. Dong et al. [135] studied (i) how the MMM signal from low-carbon steel varied under cyclic stress and (ii) how that from a defective 18CrNiWA specimen varied during the entire defect expansion [136]. Shi et al. [137] studied how the normal component of the MMM signal varied under tensile fatigue for defective 18CrNi4A specimens. Chen et al. [138] conducted tensile fatigue tests on no. 45 steel with dents. They found that the MMM signal first increased gradually with the number of cycles, then stabilized, and finally increased rapidly until fracture. Leng et al. [139] studied how the MMM signal varied during tension fatigue for no. 45 steel with V-groove defects; the results showed that local shaping strain or microscopic damage could cause nonlinear changes in the MMM

signal. Xing et al. [140] conducted fatigue tests on Q235 steel with rectangular defects; the results showed that the gradient tensor of the MMM signal was effective for characterizing the degree of damage in the ferromagnetic material. Huang et al. [141–144] measured the MMM signal from Q345 steel during crack propagation under cyclic compressive stress. Li et al. [145] studied how the MMM signal from the surface of no. 45 steel with penetrating flaws varied during fatigue loading, as shown in Fig. 34. The MMM signal increased gradually with the number of loadings and turned over when the specimen break. Kolarik et al. [146] combined the MMM method and the magnetic Barkhausen method to examine the fatigue behavior of S355J2G3 steel with rectangular grooves. Li

**Fig. 34** Change of MMM signal with cyclic loading times: **a** tangential components; **b** normal components [145]. Copyright @ 2015 Journal of Magnetism & Magnetic Materials



et al. [147] conducted an experimental study of the MMM signals from X80 pipe steel during fatigue.

### 5.2.3 Fatigue Tests Under Other Loading and Signals Evolution

The above experiments were focused mainly on fatigue under tension and compression. However, researchers have also conducted fatigue tests under bending and torque. Hu et al. [148] studied how the MMM signals from specimens with grooves varied during bending fatigue. Huang et al. [149, 150] measured and analyzed the MMM signal from structural steel undergoing dynamic bending during the propagation of fatigue cracks. Leng et al. [151] measured the MMM signal from the surface of a non-defective specimen of no. 45 steel in a bending fatigue test, and the results are shown in Fig. 35. It can be seen that the amplitude and slope of the normal component of the MMM signal decreased gradually and then increased with the number of bending loadings. Subsequently, Xu et al. [152, 153] also studied how the MMM signal from specimens of no. 45 steel with flaws varied with the number of bending loadings and how the MMM signals from non-defective Q235 steel specimens varied under tensile fatigue. Li et al. [154] studied the MMM signal from 1045 steel under rotational torque, and Hu et al. [155] studied the MMM signal from 35CrMo steel during four-point bending fatigue. Qian et al. [156] established an interface force-magnetic constitutive model based on Timoshenko beam theory and the Jiles magnetization constitutive relation, and they explained the MMM signal caused by an interfacial crack under a three-point bending load. Moreover, Qian and Huang [157] further established a fatigue cohesive zone-magnetomechanical coupling model to evaluate the interfacial crack. The model confirms that the interfacial crack propagation length  $a$  and the maximum magnetic field intensity  $H_{max}$  both increase with increasing loading cycles.

In addition, Bao et al. [158–162] studied how the magnetic induction intensity measured near the surface of steel

**Fig. 35** Changes in MMM signal with number of bending cycles under a bending moment of **a** 17.4 Nm and **b** 20.4 Nm [151]. Copyright © 2009 NDT & E International

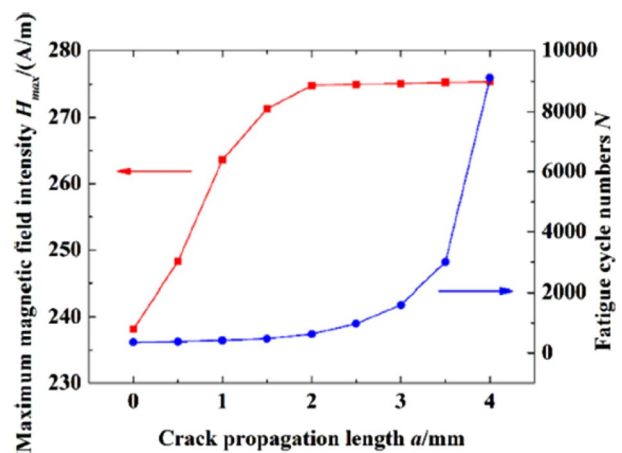
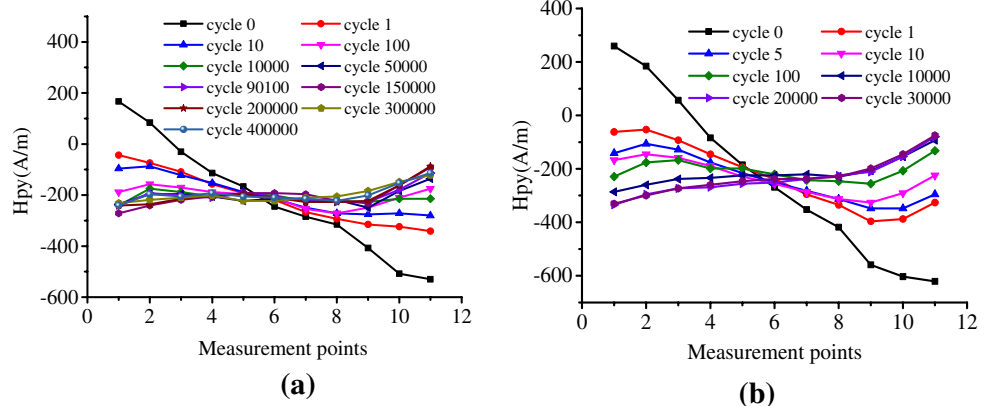


**Fig. 36** Relationship among interfacial crack propagation length  $a$ , maximum magnetic field intensity  $H_{max}$  and fatigue cycle numbers  $N$

varies under strain control fatigue loading, as shown in Fig. 36. Bao et al. [163] measured the magnetic induction during the fatigue loading of specimens, as shown in Fig. 37. The results showed that the curve of strain (stress) versus magnetic induction strength at any point near the material surface was a loop during any cyclic loading. With more cyclic loadings, the magnetic induction intensity at any point increased rapidly and then stabilized. As such, the magnetic induction characterizes well the three stages of cyclic fatigue of ferromagnetic materials.

### 5.3 Natural Magnetization Method

In 1997, a research team at the Japan Nuclear Energy Research and Development Agency found that after introducing fatigue cracks in SUS304 austenitic stainless steel, no artificial magnetic field was applied to the external magnetic field and a significant change in magnetic field was detected near the crack. That is, magnetization induced by fatigue damage occurred in the material [164]. Chen et al. [164–167] conducted theoretical and experimental research



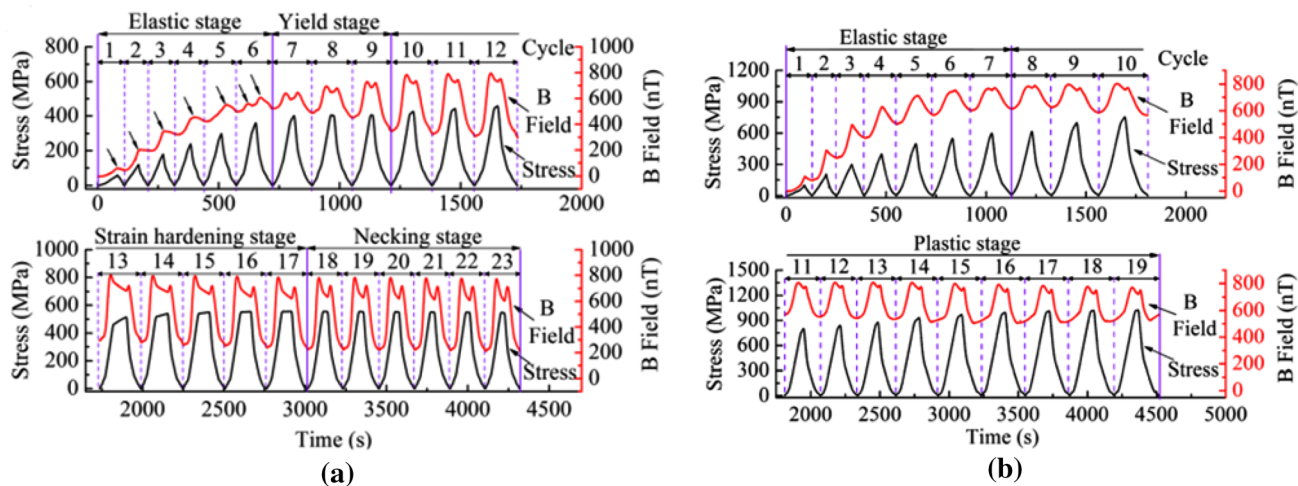


**Fig. 37** Variation of magnetic induction intensity with number of stress loadings: **a** Q345 steel; **b** U75V steel [163]. Copyright © 2016 Experimental Mechanics

into this magnetization induced by damage in austenitic stainless steel. They applied different plastic deformations and fatigue damage to specimens of no. 304 austenitic stainless steel and used ultra-small fluxgate sensors to measure how the leakage magnetic field changed in the vicinity of the specimen after loading/unloading. The results showed that for large plastic deformation, a local austenite–martensite (magnetic) phase transition occurred at the cross-slip point in SUS304 stainless steel, which may have been the inducement of magnetization by austenitic stainless-steel damage. Based on the method of magnetic-charge-distribution inversion, the correlation among damage distribution, damage degree, and magnetic-charge distribution and amplitude was studied.

The mechanisms whereby magnetization is induced by damage in austenitic stainless steel and ordinary carbon steel may be quite different. Li et al. [166] studied the relationship between the induced magnetic field and different forms and degrees of damage. They analyzed by various means how plastic deformation affected the damage-induced

magnetization, and investigated how the magnetic environment influenced the damage-induced magnetic field. In particular, they established the relationship between plastic deformation and the ferromagnetic martensitic phase content induced by deformation under experimental conditions, and found a linear correlation between the deformation-induced ferromagnetic martensite phase content and the damage-induced magnetization amplitude as shown in Fig. 38. This work shows that the degree of damage to austenitic stainless-steel materials can be detected and evaluated by detecting the strength of the natural-magnetization leakage magnetic field. They also proposed various nondestructive testing methods [168] for testing the mechanical damage in austenitic stainless-steel materials.

**Fig. 38** Relationship between magnetic charge amplitude and **a** martensite content induced by damage and **b** local maximum deformation [166]. Copyright © 2011 Journal of Applied Physics

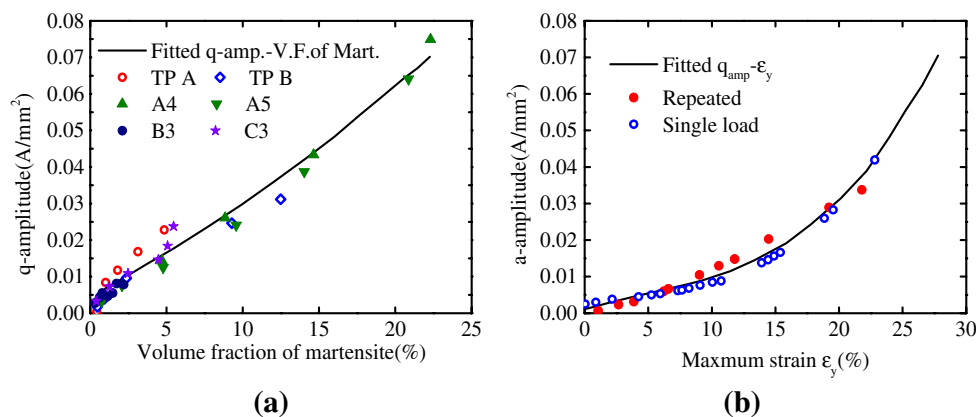
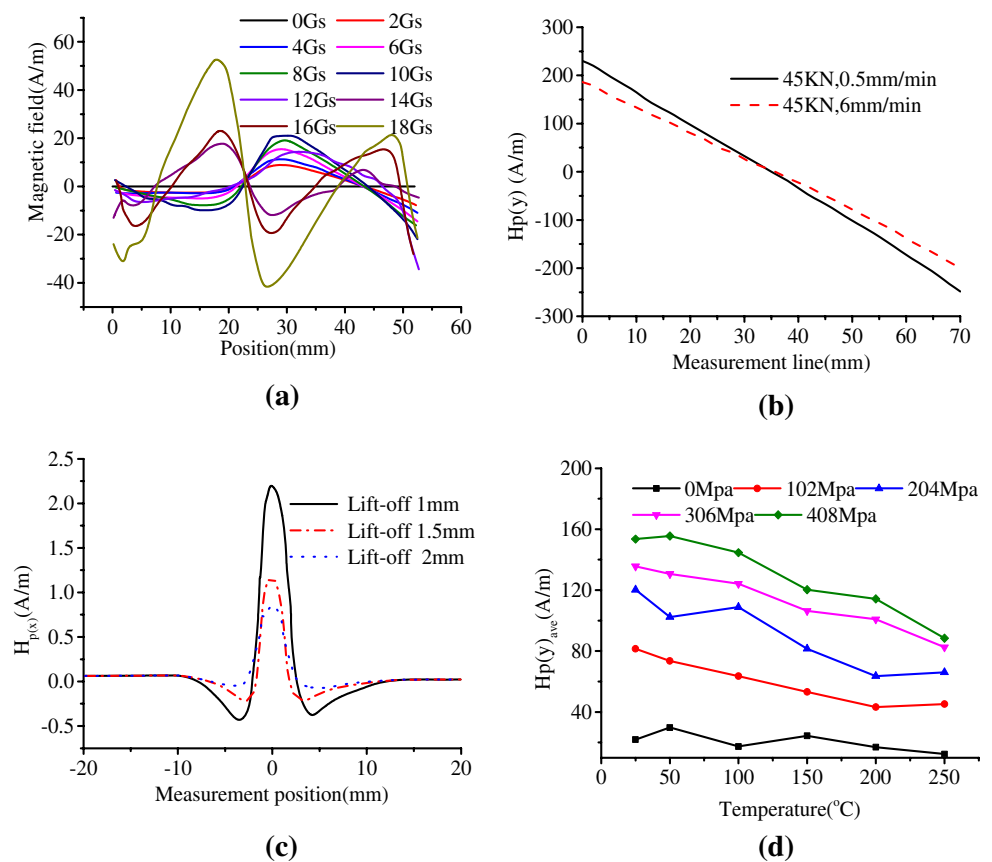


**Fig. 39** Factors affecting MMM signals: **a** environment magnetic field; [170] Copyright @2010 Nondestruct Test Evaluation; **b** loading speed; [172] Copyright @2015 Insight Nondestruct Test Condition Monitor; **c** lift-off value; [117] Copyright @ 2012 Nondestructive Testing **d** temperature [174]. Copyright @ 2016 IEEE Transactions on Magnetics



## 6 Problems and Research Trends

### 6.1 Influencing Factors

Many factors influence MMM signals, and there has also been experimental research into those factors. Yan et al. [169] designed an experiment to study how the detection time-interval and position influence the MMM signal; the results showed that while the detection time interval had no effect on the MMM signal, the signal different greatly according to the detection position. Zhong et al. [170] and Hu et al. [171] studied how environmental magnetic fields affect MMM signals; they concluded that the MMM signal from a ferromagnetic material under a given stress will invert as the environmental magnetic field gradually increases, as shown in Fig. 39a. Bao et al. [172, 173] found that the MMM signal from U75V steel depended on not only the existing damage state but also the plastic deformation caused by the load history; as shown in Fig. 39b, they found that the loading speed also affected the MMM signal measured near the surface of the specimen. Li et al. [117] designed an experiment to study how the lift-off value affects the MMM signal, as shown in Fig. 39c; the amplitude of the MMM signal from the surface of the test piece decreases gradually with the lift-off value. Recently,

Huang et al. [174] showed experimentally that temperature is another key factor affecting MMM signals, as shown in Fig. 39d. Xu et al. [175] studied experimentally how welding-defect depth, stress state, and heat-treatment type influence the MMM signal, and Singh et al. [176] showed that the deformation-induced MMM signal is influenced also by shot peening.

Therefore, a key aspect that is restricting further development of the MMM method is how to avoid the interference of external environmental factors and thereby obtain an MMM signal that reflects accurately the location and degree of the damage in ferromagnetic materials. In summary, although experiments have shown that many factors affect MMM signals, the current theoretical models of MMM signals are not effective at describing how temperature, initial magnetization, and loading speed affect MMM signals. Therefore, further study is necessary of multi-field coupling constitutive relation and quantitative theories of MMM signals in complex detection environments.

### 6.2 Quantitative Identification of Defects

It is necessary to determine whether a ferromagnetic structure contains defects, and the defect size and morphology must be given accurately to confirm whether the structure

**Table 5** Comparison of several inversion methods

Inversion method	Inversion parameters	Sample size	Inversion speed	Inversion accuracy	Other
Mapping methods					
Linear mapping method	Only applicable to single-parameter inversion	Large	Very fast	Depends on accuracy of mapping function	Not suitable for multi-parameter inversion
Neural networks method	Suitable for multi-parameter inversion	Large	Very fast	Depends strongly on level of neural network constructed	Signal noise can seriously affect inversion accuracy
Optimization inversion methods					
Stochastic optimization algorithm	Suitable for multi-parameter inversion	Small	Slow	Depends on search range and search step length	Calculation amount increases exponentially with number of inversion parameters
Gradient optimization algorithm	Suitable for multi-parameter inversion	Small	Fast	Fast convergence and high accuracy	Small changes in computational complexity caused by increase of inversion parameters, and small influence of signal noise on inversion results

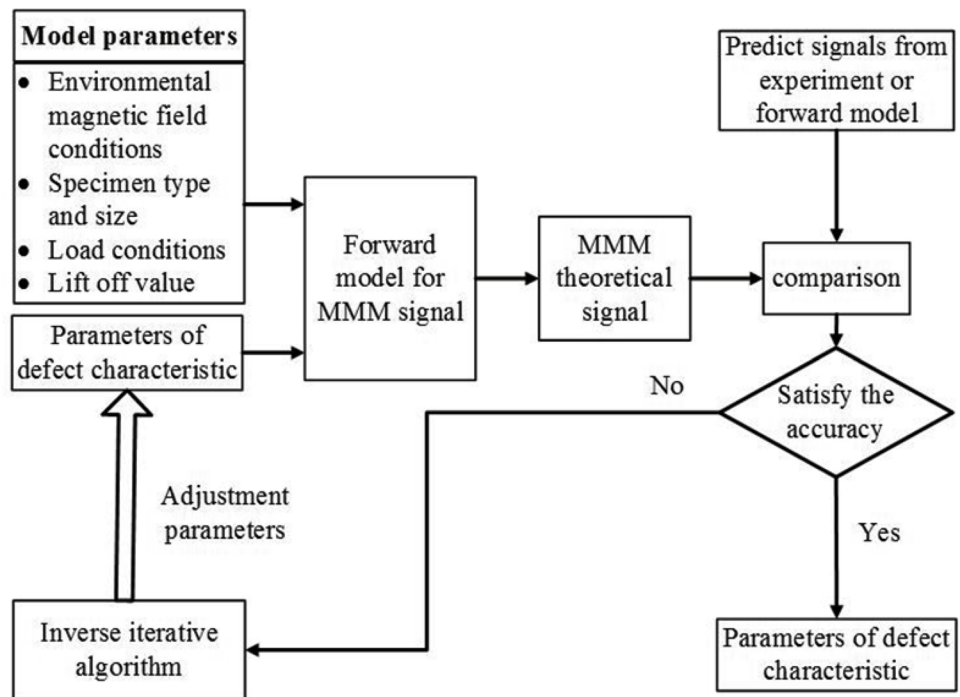
is safe. A basic problem in quantitative MMM research is quantitative analysis of the location and size of defects based on MMM signals. Table 5 summarizes the progress that has been made in quantifying defects using electromagnetic non-destructive testing methods.

The most direct method for determining defects quantitatively is linear mapping, but that method has been found to be unsuitable for the combined changes of multiple defect parameters [177]. This is because the linear relationship between defect parameters and signal characteristics is no longer satisfied when multiple defect parameters change together. When there are multiple defect parameters, the relationship between those parameters and the signal characteristics becomes more complicated, in which case intelligent algorithms such as neural networks [178] and machine learning [179, 180] are commonly used. Relevant research results show that when a neural network is used to construct the mapping relationships, the inversion accuracy depends on the level of neural network constructed strongly, and the signal noise that is inevitable in practice can seriously affect the inversion accuracy.

In addition, researchers often use optimization inversion methods to determine defects quantitatively, as shown in Fig. 40. By using an optimization algorithm, the defect parameters can be adjusted to minimize the error between the theoretical signals and the prediction signals, whereupon the defect parameters can be evaluated theoretically. Researchers have established various algorithms for solving the inverse problem of electromagnetic nondestructive testing methods such as the magnetic-flux-leakage testing method and the eddy-current testing method. The commonly used optimization inversion method is a stochastic optimization algorithm such as a genetic algorithm [181], Bayesian estimation [182], particle swarm algorithm [183, 184], the Monte Carlo Markov-chain algorithm of Bayesian theory [185]. When these stochastic optimization algorithms perform inversion analysis on the defect parameters, the inversion result depends on the search range and the search step length, and the amount of calculation increases exponentially with the number of inversion parameters. In addition, other important methods for solving the inverse problem are based on the gradient optimization algorithm [186–191]. These inversion methods are compared in Table 5. Compared with other algorithms, the gradient optimization algorithm has the advantages of (i) being suitable for multi-parameter inversion, (ii) having fast convergence and high accuracy, (iii) undergoing small changes in computational complexity with more inversion parameters, and (iv) signal noise having a little influence on the inversion results.

Chen et al. used the conjugate-gradient iterative algorithm to study systematically the reconstruction of the complex defect topography encountered in eddy-current testing and magnetic-flux-leakage detection. The flow of this algorithm

**Fig. 40** Inversion problem-solving process. Copyright © 2018 IEEE Transactions on Magnetics



is shown in Fig. 40. However, for the lack of quantitative quantification of MMM methods, it remains impossible to analyze quantitatively the extent, morphology, and size of stress-concentration areas or defects, which seriously restricts the application of MMM methods in engineering. Analyzing the gradient iterative algorithm proposed by Chen et al. [188] shows that it cannot guarantee that the search direction satisfies the conjugate feature, and the values of the iterative parameters in the defect topology estimation affect the convergence of the iterative algorithm. Shi et al. [25] established a method for reconstructing the identification of stress and defects based on conjugate-gradient inversion and described the inversion problem of the MMM method in detail. The objective function to be optimized for the inversion problem was determined and an iterative algorithm for inversion was established. In combination with

previous MMM experimental signal reconstruction analysis of defects, it was confirmed that a hole defect of 6 mm in radius could be effectively reconstructed using the MMM signal, as shown in Fig. 41. In particular, the feasibility of quantifying early damage using MMM signals was verified for the first time. To date, researchers have conducted only preliminary studies of the quantitative identification of stress and defects, and further relevant quantitative research is needed. Such researches will have important theoretical and practical significance for promoting the application of MMM methods.

**Fig. 41** Inversion analysis of size and location of circular hole defect: **a** inversion results and MMM experimental signals; **b** true, initial, and reconstructed defect morphology [25]. Copyright © 2018 IEEE Transactions on Magnetics

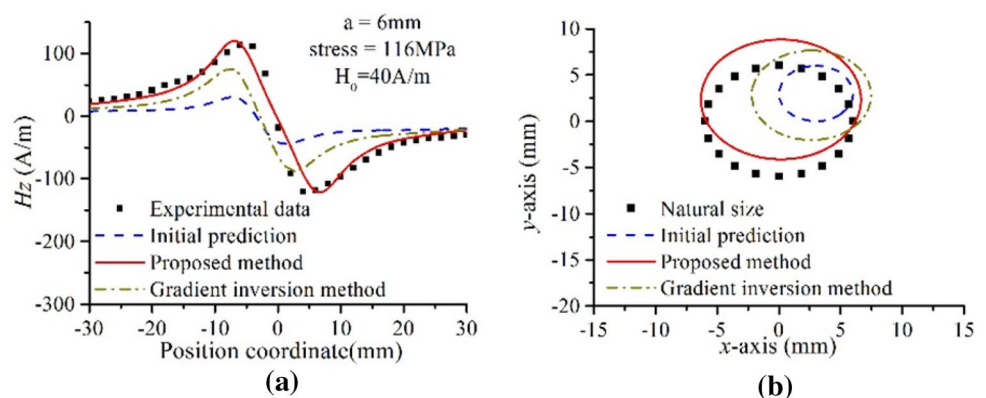


**Fig. 42** Disk rims detection and stress concentration induced MMM signal. **a** Schematic arrangement for checking disk rims. **b** Typical distribution of the residual magnetization field  $H$  along the disk rim [192]. Copyright@2010, Thermal Engineering

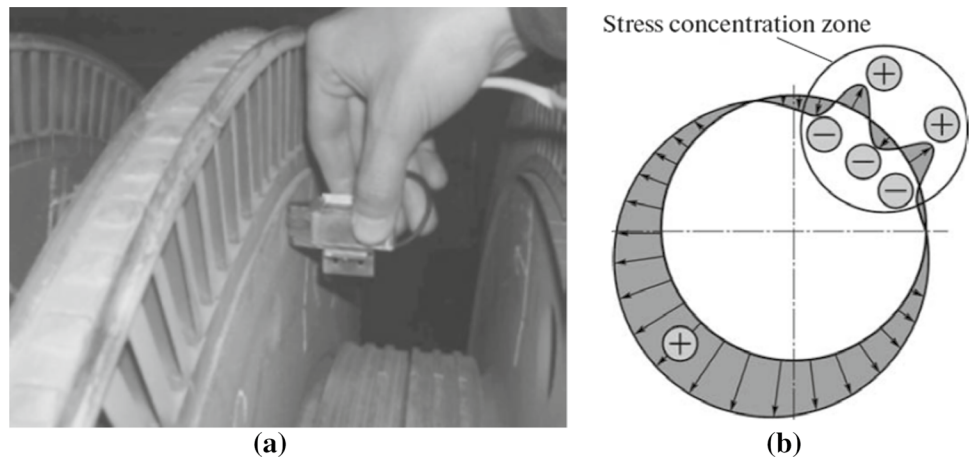


**Fig. 43** Assessment of the material state and weld quality. **a** Execution of gas pipeline testing. **b** Weld inspection procedure [195] Copyright@2012, Welding in the World



### 6.3 MMM Applications

The method of MMM testing has been widely used as a strictly defect detection method focused on finding the existing material discontinuities, and has been used to define the areas in the component which are most prone to the potential development of discontinuities. The MMM method has been widely used in residual life assessment and engineering inspection of the power equipment, oil and gas pipeline, chemical industry; metal structures; mechanical engineering and other fields.

Dubov [192] presented a comprehensive examination of blade slots, disks, blade roots, and their attachment assemblies using the MMM method. As shown in Fig. 42a, the checking scheme according to disk rims and Fig. 42b given the typical distribution of the MMM field in the stress concentration zone revealed on the disk rim in the all forged part of a rotor. The experimental results confirmed the good efficiency of using MMM methods. Dubov and his colleagues [193–195] considered the possibilities for the application of the MMM method for assessment of the stress–strain state and non-destructive testing of oilfield pipeline and gas pipelines, as shown in Fig. 43. Li et al. [196] studied the calculation scheme of MMM signal for pipeline defect detection

with a relatively large lift-off distance based on magnetic dipoles. By comparing the calculation results with the measured signals, the phenomenon of signal abruptness caused by defects was initially explained. Liu et al. [197–199] studied the application of MMM method in the internal stress damage and axial crack in long-distance oil and gas pipelines.

Gear is the basic component of a mechanical transmission system. The detection of gear cracks is critical to ensuring the safety and reliability of the entire mechanical transmission system. Kang et al. [200] studied the application of MMM method in gear micro crack detection. Based on the static testing and dynamic detection with load, the detection position and load effect on detection results of micro crack on the side of an actual gear are analyzed. Roskosz and his colleagues [201–203] investigated how to use MMM method to find defects of the toothed gears in the early stages of the development. Figure 44 shows the actual toothed gears after failure and its MMM signal. Studies have shown that there are some correlations between the number of cycles of load change, the value of the load and the distribution on the tooth width, and the value of the magnetic field component. And then, some symptoms of anticipated dental fatigue damage can be observed in the distribution of MMM signal.

Welding technology is an indispensable processing technology in high-quality and high-efficiency manufacturing technology in modern industry. Non-destructive testing of welding quality based on MMM method has been applied to ensure the safe operation of welded structures. Dubov and Kolokolnikov [204, 205] carried out comprehensive MMM testing of base metal and welded joints of welded steel structures and steam turbine parts, as shown in Fig. 45. By comparing with the small hole stress testing method, Li et al. [206] demonstrated that the

magnetic field abnormality near the ferromagnetic material surface could be used for residual stress inspection of a welding seam in the tube specimen. Li et al. [207] introduced a method based on continuous wavelet transform energy spectrum to analyze the locating of welding cracks. Yang et al. [208] carried out the fatigue tests for Q345B and Q345qC welding and non-welding specimens and tested the MMM signal. Qi et al. [209] used the MMM technique to locate the region with high residual stress, and tested the stress in a welded steel ship plate based on

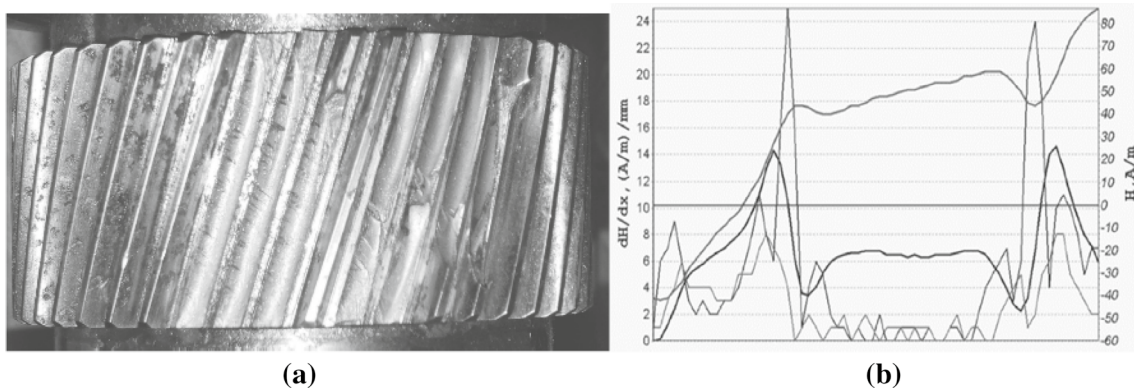


Fig. 44 The actual toothed gears after failure (a) and its MMM signal (b) [201], Copyright@2010, Journal of achievements in materials and manufacturing engineering

Fig. 45 Testing scheme of welded joint by using a special scanning device. a The three components measurement of the MMM signal, b special scanning device for testing of welded joints [204] Copyright@2014, Welding in the World

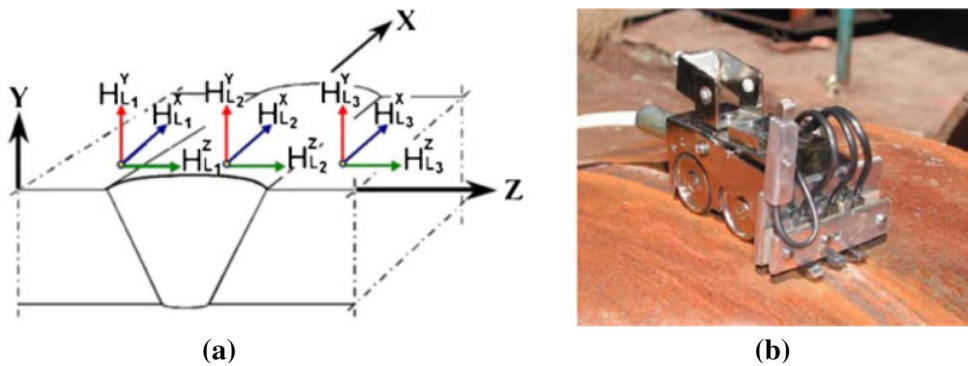
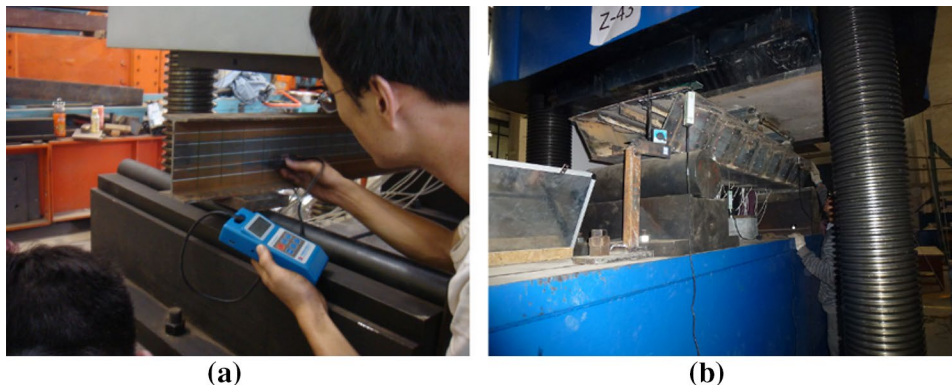
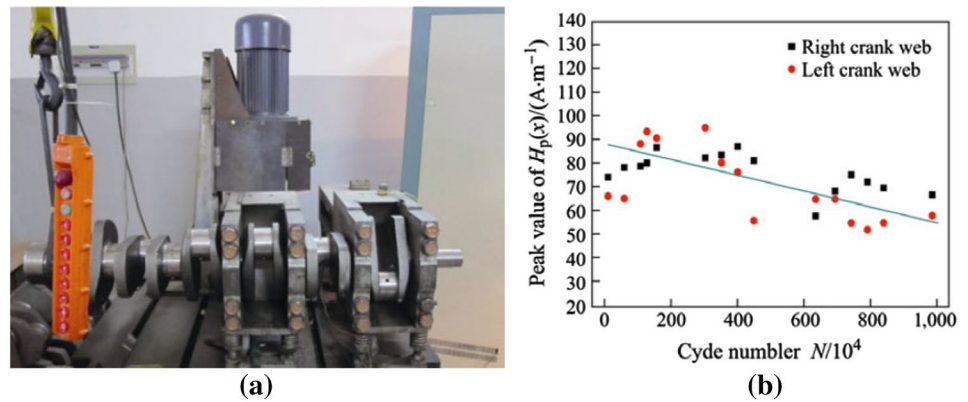


Fig. 46 Measurement of MMM signal for Civil steel structure (a) a steel beam testing [212], Copyright@2016, The Structural Design of Tall and Special Buildings (b) a inclined steel box girder testing [213], Copyright@2020, International Journal of Applied Electromagnetics and Mechanics



**Fig. 47** Life prediction of crankshaft remanufacturing core. **a** Photo of resonance bending fatigue test machine for Crankshaft. **b** Variations of peak value of Hx parameters of MMM signals with the cycles [214] Copyright@2013, Advances in Manufacturing



the magnetic Barkhausen Noise technique. Su et al. [210] measured the normal component of the MMM field for the defective and non-defective butt welded Q345 steel specimens.

The MMM method has been also applied to the non-destructive testing of metal structures in mechanical and civil engineering and other fields. Agnieszka et al. [211] considered the continuous inspection of crane's structure using the MMM method, and analyzed the influence of varying load and trolley position on the MMM signal components. Wang et al. [212] measured the MMM signals of four-point flexural tests under different loads for a flange and web of a steel beam, as shown in Fig. 46a. As shown in Fig. 46b, Su et al. [213] carried out a four-point bending tests for a inclined steel box girder to distinguish the effect of normal stress and shear stress on MMM field. Dong et al. [214] carried out a bending fatigue bench tests to collect MMM signal during fatigue process, as shown in Fig. 47. In addition, Lesiak and Radziszewski [215, 216] discussed the application of the MMM method in rail transport.

## 7 Conclusions

As a nondestructive testing technology, the MMM method has been under development for over 20 years. It has shown excellent application prospects in early diagnosis and life prediction for ferromagnetic components, and it has been recognized widely by experts and researchers. To date, researchers from all over the world have made some progress in theoretical research, instrument and equipment research and development, experimental research, damage assessment, and engineering inspection applications of the MMM method. However, the method still has many problems to be solved in the analysis of influencing factors, detection repeatability and reliability, and quantitative evaluation. (1) Systematic research is still needed on the theoretical system of the MMM method, as does on the corresponding

quantitative relationship between the MMM signal and the defect geometry for use in detection. (2) Experiments have shown that many factors affect MMM signals. To date, theoretical models of MMM signals cannot yet consider fully the combined effects of temperature, environmental magnetic field, initial magnetization, loading form, and other factors on the MMM signal. (3) Existing criteria for damage determination often fail in practical applications. One of the main reasons is that because the tested structure is often subjected to long-term cyclic loading in actual situations, the MMM signal and its characteristic quantity both change with the number of cycles.

Given the current research problems, follow-up studies are required. (1) There is an urgent need to establish a systematic and complete theoretical system for the MMM method, from magnetomechanical modeling based on microscopic phenomena to quantitative analysis of macroscopic MMM signals and finally to quantitative evaluation of residual stress/defects for inspection-oriented applications. (2) More research is needed into the multi-field coupled constitutive relation and a quantitative theory of MMM signals in complex detection environments. Research is also needed into how temperature, the external magnetic environment, loading form and velocity, initial magnetization, elasto-plastic state, and other factors influence the MMM signal, as well as the physical mechanism whereby these factors are coupled. (3) An in-depth quantitative theoretical study is required of how MMM signals evolve during fatigue, whereupon the MMM detection data obtained during a long fatigue process could be described quantitatively. In combination with the law for how MMM signals evolve and using the correlation of data in the fatigue process to predict how the damage develops, some new criterion of the MMM method for damage considering fatigue would be developed, and this would greatly improve the practical applicability of the method.

The MMM method is a nondestructive testing method that can detect early damage in a material, and it has wide application prospects. Continued pioneering in-depth

studies are expected to make more breakthroughs in the detection mechanism of the MMM method, the establishment and extraction of MMM signal features, and quantitative evaluation and damage assessment. These advances will allow the MMM method to contribute fully to the early damage pre-diagnosis of ferromagnetic materials and enable the method to better serve engineering applications. In addition, taking this opportunity of studying the MMM method will promote the development of applied physics, ferromagnetics, mechanics, nondestructive testing, and other disciplines.

**Acknowledgements** This work was supported by the Natural Science Foundation of China [Grant Nos. 11802225] and the Natural Science Basic Research Plan in the Shaanxi Province of China [Program Nos. 2019JQ-261]. We also thank two anonymous reviewers for their helpful comments on an earlier draft of this paper. Particularly, Dr. Pengpeng Shi is deeply indebted to his supervisor Professor Xiaojing Zheng, who encouraged the author to write this review and provided some important guidance.

## References

- Jiles, D.C.: Review of magnetic methods for nondestructive evaluation. *NDT Int* **23**(2), 83–92 (1990)
- Yao, Y., Tung, S.T.E., Glisic, B.: Crack detection and characterization techniques: an overview. *Struct Control Health Monitor* **21**(12), 1387–1413 (2014)
- Adevale, I.D. Multiple parameters based pulsed eddy current non-destructive testing and evaluation (2015)
- Coramik, M., Ege, Y.: Discontinuity inspection in pipelines: a comparison review. *Measurement* **111**, 359–373 (2017)
- Felice, M.V., Zheng, F.: Sizing of flaws using ultrasonic bulk wave testing: a review. *Ultrasonics* **88**, 26–42 (2018)
- Suzuki, M., Komura, I., Takahashi, H.: Nondestructive estimation of residual stress in welded pressure vessel steel by means of remanent magnetization measurement. *Int J Pres Ves Pip* **6**(2), 87–112 (1978)
- Atherton, D., Coathup, L., Jiles, D., et al.: Stress induced magnetization changes of steel pipes: laboratory tests. *IEEE Trans Magn* **19**(4), 1564–1568 (1983)
- Atherton, D., Welbourn, C., Jiles, D., et al.: Stress-induced magnetization changes of steel pipes: laboratory tests Part II. *IEEE Trans Magn* **20**(6), 2129–2136 (1984)
- Atherton, D.L., Jiles, D.C.: Effects of stress on magnetization. *NDT Int* **19**(1), 15–19 (1986)
- Dubov, A.A.: A study of metal properties using the method of magnetic memory. *Metal Sci Heat Treat* **39**(9), 401–405 (1997)
- Shi, P.P., Zheng, X.J.: Magnetic charge model for 3D MMM signals. *Nondestruct Test Eval* **31**(1), 45–60 (2016)
- Jiles, D.C.: Theory of the magnetomechanical effect. *J Phys D* **28**(8), 1537–1546 (1995)
- Wang, Z.D., Gu, Y., Wang, Y.S.: A review of three magnetic NDT technologies. *J Magn Magn Mater* **324**(4), 382–388 (2012)
- Bao, S., Fu, M.L., Hu, S.N., Gu, Y.B., Lou, H.J.: A review of the metal magnetic memory technique. *ASME 2016 35th International Conference on Ocean, Offshore and Arctic Engineering* (2016). <https://doi.org/10.1115/OMAE2016-54269>
- Shen, G.T., Hu, B., Xu, Y.C., et al.: *China Non-destructive Testing 2025 Technology Development Strategy*. Standards Press of China, Beijing (2017)
- Dubov, A.A.: Development of a metal magnetic memory method. *Chem Petrol Eng* **47**(11–12), 837–839 (2012)
- Tanasienko, A.G., Sunstov, S.I., Dubov, A.A.: Monitoring chemical plant by a metal magnetic memory method. *Chem Petrol Eng* **38**(9–10), 624–629 (2002)
- Kuleev, V.G., Dubov, A.A., Lopatin, V.V.: Zero-level lines of scattered field on surfaces of ferromagnetic steel pipes with flaws. *Russ J Nondestruct Test* **38**(5), 343–356 (2002)
- Dubov, A.A.: Detection of metallurgical and production defects in engineering components using metal magnetic memory. *Metallurgist* **59**(1–2), 164–167 (2015)
- Pengpeng, S.: Quantitative study of micro-magnetic nondestructive testing for stress and defect in ferromagnetic materials. Xidian University, China, Thesis (2017)
- Joule, J.P.: On a new class of magnetic forces. *Ann. Electr. Magn. Chem* **1842**(8), 219–224 (1842)
- Villari, E.: Change of magnetization by tension and by electric current. *Ann. Phys. Chem* **126**, 87–122 (1865)
- Jiles, D.: *Introduction to Magnetism and Magnetic Materials*. CRC Press, Boca Raton (2015)
- Zhang, P., Liu, L., Chen, W.M.: Analysis of characteristics and key influencing factors in magnetomechanical behavior for cable stress monitoring. *Acta Phys. Sin.* **62**(17), 177501–177501 (2013)
- Shi, P.P., Jin, K., Zhang, P.C., et al.: Quantitative inversion of stress and crack in ferromagnetic materials based on metal magnetic memory method. *IEEE Trans. Magn.* **54**(10), 6202011 (2018)
- Craik, D.J., Wood, M.J.: Magnetization changes induced by stress in a constant applied field. *J. Phys. D Appl. Phys.* **3**(7), 1009 (1970)
- Jian, X.L., Jian, X.C., Deng, G.Y.: Experiment on relationship between the magnetic gradient of low-carbon steel and its stress. *J. Magn. Magn. Mater.* **321**(21), 3600–3606 (2009)
- Long, F.F., Wang, J.Z., Gao, G.Z., et al.: Tempering effect and tensile properties evaluation of C45 steel based on magnetic memory technology. *Mater. Eval.* **72**(11), 1414–1420 (2014)
- Shui, G.S., Li, C.W., Yao, K.: Non-destructive evaluation of the damage of ferromagnetic steel using metal magnetic memory and nonlinear ultrasonic method. *Int. J. Appl. Electromagn. Mech.* **47**(4), 1023–1038 (2015)
- Chen, S.L., Pang, Y., Tang, Y.L., et al.: Metal magnetic memory testing method of multiple lift-off values. *Nanotechnol. Prec. Eng.* **14**(6), 421–428 (2016)
- Chen, H.L., Wang, C.L., Zhu, H.Y.: Metal magnetic memory test method based on magnetic gradient tensor. *Chin. J. Sci. Instrum.* **37**(3), 602–609 (2016)
- Xu, K.S., Qiu, X.Q., Tian, X.S.: Theoretical investigation of metal magnetic memory testing technique for detection of magnetic flux leakage signals from buried defect. *Nondestruct. Test Eval.* **33**(1), 45–55 (2017)
- Su, H., Chen, M.: Magnetic memory signal changes of 45# steel in the process of fatigue. *Int. J. Appl. Electromagn. Mech.* **52**(3), 1623–1628 (2016)
- Payne, M.A.: SI and Gaussian CGS units, conversions and equations for use in geomagnetism. *Phys. Earth Planet. Inter.* **26**, P10–P16 (1981)
- Lin, J.M., Sha, H.: A new nondestructive testing technique based on magnetic memory effect. *Nondestruct. Test* **22**(7), 297–299 (2000)
- Huang, S.L., Li, L.M., Wang, L.F., et al.: Stress distribution testing by metal magnetic memory method. *Nondestruct. Test* **24**(5), 212–214 (2002)



37. Zhang, W.M., Doubov, A.A., Sun, H.T., et al.: The metal magnetic memory phenomenon of high-strength steel in the process of grinding. *Acta Armamentarii* **26**(03), 375–378 (2005)
38. Wilson, J.W., Gui, Y.T., Barrans, S.: Residual magnetic field sensing for stress measurement. *Sensor Actuat. A-Phys.* **135**(2), 381–387 (2007)
39. Doubov, A.A. Physical base of the method of metal magnetic memory – own magnetic field of dislocations. Conference Proceedings AMAS. Centre of Excellence for Advanced Materials and Structures 2, 1–9 (2002)
40. Ren, J.L., Chen, C., Liu, C.K., et al.: Experimental research on microcosmic mechanism of stress-magnetic effect for magnetic memory testing. *J. Aeronaut. Mater.* **28**(5), 41–44 (2008)
41. Qiu, F.S., Ren, W., Tian, G.Y., Gao, B.: Characterization of applied tensile stress using domain wall dynamic behavior of grain-oriented electrical steel. *J. Magn. Magn. Mater.* **432**, 250–259 (2017)
42. Qiu, F.S., Klug, M.J., Tian, G.Y., Hu, P., McCord, J.: Influence of magnetic domain wall orientation on Barkhausen noise and magneto-mechanical behavior in electrical steel. *J. Phys. D Appl. Phys.* **52**, 265001 (2019)
43. Bao, S., Liu, X., Zhang, D.: Variation of residual magnetic field of defective U75V steel subjected to tensile stress. *Strain* **51**(5), 370–378 (2015)
44. Yao, K.: Experimental Research on Testing and Evaluation of Early Damage of Ferromagnetic Materials Based on Metal Magnetic Memory Method. Beijing Jiaotong University, Beijing (2014)
45. Roskosz, M., Gawrilenko, P.: Analysis of changes in residual magnetic field in loaded notched samples. *NDT&E Int.* **41**(7), 570–576 (2008)
46. Guo, P.J., Chen, T., Lian, X.M., et al.: Detection of cracks in 25Cr35NiNb ethylene pyrolysis furnace tubes by metal magnetic memory technique. *J. Press. Vess. Technol.* **139**(2), 024501 (2017)
47. Leng, J.C., Xu, M.Q., Li, J.W., et al.: Characterization of the elastic-plastic region based on magnetic memory effect. *Chin. J. Mech. Eng.* **23**(4), 532–536 (2010)
48. Dong, L.H., Xu, B.S., Dong, S.Y., et al.: Metal magnetic memory signals from surface of low-carbon steel and low-carbon alloyed steel. *J. Cent. South Univ. Technol.* **14**(1), 24–27 (2007)
49. Dong, L.H., Xu, B.S., Dong, S.Y., et al.: Variation of stress-induced magnetic signals during tensile testing of ferromagnetic steel. *NDT&E Int.* **41**(3), 184–189 (2008)
50. Dong, L.H., Xu, B.S., et al.: Stress dependence of the spontaneous stray field signals of ferromagnetic steel. *NDT&E Int.* **42**(4), 323–327 (2009)
51. Shi, C.L., Dong, S.Y., Xu, B.S., et al.: Metal magnetic memory effect caused by static tension load in a case-hardened steel. *J. Magn. Magn. Mater.* **322**(4), 413–416 (2010)
52. Bao, S., Lin, L., Zhang, D., et al.: Characterization of stress-induced residual magnetic field in ferromagnetic steel. 34th International Conference on Ocean, Offshore and Arctic Engineering. American Society of Mechanical Engineers, V004T03A029-V004T03A029 (2015)
53. Huang, H.H., Yang, C., Qian, Z.C., et al.: Magnetic memory signals variation induced by applied magnetic field and static tensile stress in ferromagnetic steel. *J. Magn. Magn. Mater.* **416**, 213–219 (2016)
54. Shi, P.P., Jin, K., Zheng, X.J.: A magnetomechanical model for the magnetic memory method. *Int. J. Mech. Sci.* **124**, 229–241 (2017)
55. Ren, S.K., Ren, X.Z.: Studies on laws of stress-magnetization based on magnetic memory testing technique. *J. Magn. Magn. Mater.* **499**, 165–171 (2018)
56. Zhang, W.M., Liu, H.G., Yuan, J.J., et al.: Change of weak magnetic signals and metal magnetic memory effects during the torsion of low carbon steel. *Trans Beijing Inst. Technol.* **25**(11), 1003–1007 (2005)
57. Xing, H.Y., Fan, J.M., Li, X.F., et al.: Bend deformation state of ferromagnetic materials based on metal magnetic memory theory. *J. Harbin Inst. Technol.* **38**(7), 1017–1019 (2006)
58. Roskosz, M., Bieniek, M.: Evaluation of residual stress in ferromagnetic steel based on residual magnetic field measurements. *NDT&E Int.* **45**(1), 55–62 (2012)
59. Roskosz, M., Bieniek, M.: Analysis of the similarity between residual magnetic field distribution and the stress and strain state for 7CrMoVTiB10–10 (T/P24) steel. *Int Symp Appl Electro-magn Mech* 521–527 (2012)
60. Roskosz, M., Bieniek, M.: Analysis of the universality of the residual stress evaluation method based on residual magnetic field measurements. *NDT&E Int.* **54**(3), 63–68 (2013)
61. Hu, B., Yu, R.: Variations in surface residual compressive stress and magnetic induction intensity of 304 stainless steel. *NDT&E Int.* **80**, 1–5 (2016)
62. Yao, K., Wu, L.B., Wang, Y.S.: Nondestructive Evaluation of contact damage of ferromagnetic materials based on metal magnetic memory method. *Exper Technique* **43**(3), 273–285 (2019)
63. Li, J.W., Xu, M.Q.: Influence of uniaxial plastic deformation on surface magnetic field in steel. *Meccanica* **47**(1), 135–139 (2012)
64. Li, J.W., Liang, X.Y., Han, X.M.: Influence of applied load in ferromagnetic material on magneto-mechanical phenomena. *Insight Nondestruct Test Condition Monitor* **58**(6), 308–312 (2016)
65. Leng, J.C., Liu, Y., Zhou, G.Q., et al.: Metal magnetic memory signal response to plastic deformation of low carbon steel. *NDT&E Int.* **55**(3), 42–46 (2013)
66. Guo, P.J., Chen, X.D., Guan, W.H., et al.: Correlation between magnetic memory signals and mechanical properties of 35CrMo tempered and quenched steel. *Appl. Mech. Mater.* **750**, 186–191 (2015)
67. Usarek, Z., Augustyniak, B.: Evaluation of the impact of geometry and plastic deformation on the stray magnetic field around the bone-shaped sample. *Int. J. Appl. Electromagn. Mech.* **48**, 195–199 (2015)
68. Qiu, Z.C., Zhang, W.M., Yu, X., et al.: Monitoring yield failure of ferromagnetic materials with spontaneous abnormal magnetic signals. *Tehnički Vjesnik* **22**(4), 953–958 (2015)
69. Li, X.M., Lv, K.F., Li, G.T., et al.: Magnetic memory effect of Q235 steel under static tension condition. *Phys. Exam Test* **31**(5), 10–13 (2013)
70. Zhong, L.Q., Li, L.M., Chen, X.: Simulation of magnetic field abnormalities caused by stress concentrations. *IEEE Trans. Magn.* **49**(3), 1128–1134 (2013)
71. Yao, K., Wang, Z.D., Deng, B., et al.: Experimental research on metal magnetic memory method. *Exper. Mech.* **52**(3), 305–314 (2012)
72. Bao, S., Lou, H.J., Fu, M.L., et al.: Correlation of stress concentration degree with residual magnetic field of ferromagnetic steel subjected to tensile stress. *Nondestruct. Test Eval.* **32**(3), 255–268 (2017)
73. Li, X.M., Ding, H.S., Bai, S.W.: Research on the stress-magnetism effect of ferromagnetic materials based on three-dimensional magnetic flux leakage testing. *NDT&E Int.* **62**(2), 50–54 (2014)
74. Ren, J.L., Wang, D.S., Song, K.: Experimental study on magnetic memory effect of typical ferromagnetism items. *Nondestruct. Test.* **27**(8), 409–411 (2005)
75. Hu, B., Yu, R.Q., Zou, H.C.: Magnetic non-destructive testing method for thin-plate aluminum alloys. *NDT&E Int.* **47**, 66–69 (2012)
76. Li, Z.C., Dixon, S., Cawley, P., et al.: Experimental studies of the magneto-mechanical memory (MMM) technique using

- permanently installed magnetic sensor arrays. *NDT&E Int.* **92**, 136–148 (2017)
77. Kolokolnikov, S.M., Dubov, A.A., Marchenkov, A.Y.: Determination of mechanical properties of metal of welded joints by strength parameters in the stress concentration zones detected by the metal magnetic memory method. *Weld World* **58**(5), 699–706 (2014)
  78. Li, Z.C., Dixon, S., Cawley, P., et al.: Study of metal magnetic memory (MMM) technique using permanently installed magnetic sensor arrays. *Rev. Progress Quant. Nondestruct. Eval.* **1806**(1), 110011 (2017)
  79. Roskosz, M.: Metal magnetic memory testing of welded joints of ferritic and austenitic steel. *NDT&E Int.* **44**(3), 305–310 (2011)
  80. Bao, S., Fu, M.L., Lou, H.J., et al.: Evaluation of stress concentration of a low carbon steel based on residual magnetic field measurements. *Insight Nondestruct. Test Condition Monitor.* **58**(12), 678–682 (2016)
  81. Bao, S., Bai, S.Z., Mustapha, A., et al.: Property evaluation of Q345 welded steel by tangential residual magnetic field. *ASME 2017, International Conference on Ocean, Offshore and Arctic Engineering V004T03A038* (2017)
  82. Zheng, X.J., Liu, X.E.: A nonlinear constitutive model for Terfenol-D rods. *J. Appl. Phys.* **97**(5), 053901 (2005)
  83. Shi, P.P., Jin, K., Zheng, X.J.: A general nonlinear magnetomechanical model for ferromagnetic materials under a constant weak magnetic field. *J. Appl. Phys.* **119**(14), 14103 (2016)
  84. Yang, E., Li, L.M., Chen, X.: Magnetic field aberration induced by cycle stress. *J. Magn. Magn. Mater.* **312**(1), 72–77 (2007)
  85. Guo, P.J., Chen, X.D., Guan, W.H., et al.: Effect of tensile stress on the variation of magnetic field of low-alloy steel. *J. Magn. Magn. Mater.* **323**(20), 2474–2477 (2011)
  86. Leng, J.C., Xu, M.Q., Zhou, G.Q., et al.: Effect of initial remanent states on the variation of magnetic memory signals. *NDT&E Int.* **52**, 23–27 (2012)
  87. Ren, S.K., Ren, X.Z., Duan, Z.X., et al.: Studies on influences of initial magnetization state on metal magnetic memory signal. *NDT&E Int.* **103**, 77–83 (2019)
  88. Xu, M.X., Xu, M.Q., Li, J.W., et al.: Discuss on using Jiles-Atherton theory for characterizing magnetic memory effect. *J. Appl. Phys.* **112**(9), 093902 (2012)
  89. Li, J.W., Xu, M.Q., Leng, J.C., et al.: Modeling plastic deformation effect on magnetization in ferromagnetic materials. *J. Appl. Phys.* **111**(6), 063909 (2012)
  90. Leng, J.C., Li, L., Gao, Y.T., et al.: Modelling dependence of magnetic memory effect on plastic deformation in ferromagnetic materials. *Mater. Sci. Technol.* **30**(1), 81–85 (2014)
  91. Yao, K., Deng, B., Wang, Z.D.: Numerical studies to signal characteristics with the metal magnetic memory-effect in plastically deformed samples. *NDT&E Int.* **47**, 7–17 (2012)
  92. Shi, P.P., Zhang, P.C., Jin, K., et al.: Thermo-magneto-elastoplastic coupling model of metal magnetic memory testing method for ferromagnetic materials. *J. Appl. Phys.* **123**(14), 145102 (2018)
  93. Zeng, K., Tian, G.Y., Liu, J., et al.: Repeatability and stability study of residual magnetic field for domain wall characterization. *J. Magn. Magn. Mater.* **485**, 391–400 (2018)
  94. Pengpeng, S., Peigen, B., Chen Hong-en, Su, Sanqing, C.Z.: The magneto-elastoplastic coupling effect on the magnetic flux leakage signal. *J. Magn. Magn. Mater.* (2020). <https://doi.org/10.1016/j.jmmm.2020.166669>
  95. Pengpeng, S.: Analytical solutions of magnetic dipole model for defect leakage magnetic fields. *NDT* **37**, 1–7 (2015)
  96. Huang, H.H., Jiang, S.L., Yang, C., et al.: Stress concentration impact on the magnetic memory signal of ferromagnetic structural steel. *Nondestruct. Test Eval.* **29**(4), 377–390 (2014)
  97. Wang, Z.D., Yao, K., Deng, B., et al.: Theoretical studies of metal magnetic memory technique on magnetic flux leakage signals. *NDT&E Int.* **43**(4), 354–359 (2010)
  98. Wang, Z.D., Yao, K., Deng, B., et al.: Quantitative study of metal magnetic memory signal versus local stress concentration. *NDT&E Int.* **43**(6), 513–518 (2010)
  99. Roskosz, M., Rusin, A., Bieniek, M.: Analysis of relationships between residual magnetic field and residual stress. *Meccanica* **48**(1), 45–55 (2013)
  100. Su, S., Ma, X., Wang, W., Yang, Y.Y.: Stress-dependent magnetic charge model for micro-defects of steel wire based on the magnetic memory method. *Res. Nondestruct. Eval.* **31**(1), 24–47 (2020)
  101. Yang, L.J., Liu, B., Chen, L.J., et al.: The quantitative interpretation by measurement using the magnetic memory method (MMM)-based on density functional theory. *NDT&E Int.* **55**, 15–20 (2013)
  102. Wang, G.Q., Yan, P., Wei, L.W., et al.: The magnetic memory effect of ferromagnetic materials in the process of stress-magnetism coupling. *Adv Mater Sci Eng* 1284560 (2017)
  103. Liu, B., He, Y.Y., Zhang, H., et al.: Study on characteristics of magnetic memory testing signal based on the stress concentration field. *IET Sci. Meas. Technol.* **11**(1), 2–8 (2017)
  104. Liu, B., Fu, Y., Jian, R.: Modelling and analysis of magnetic memory testing method based on the density functional theory. *Nondestruct. Test Eval.* **30**(1), 13–25 (2015)
  105. Liu, B., Xue, X.M., Li, J.M., et al.: Grain size effect on metal magnetic memory signal for stress damage evaluation of low carbon steel. *Nondestruct. Test Eval.* **34**(3), 267–282 (2019)
  106. Liu, B., Fu, Y., Xu, B.: Study on metal magnetic memory testing mechanism. *Res. Nondestruct. Eval.* **26**(1), 1–12 (2015)
  107. Carman, G.P., Mitrovic, M.: Nonlinear constitutive relations for magnetostrictive materials with applications to 1-D problems. *J. Intell. Mater. Syst. Struct.* **6**(5), 673–683 (1995)
  108. Wan, Y.P., Fang, D.N., Hwang, K.C.: Non-linear constitutive relations for magnetostrictive materials. *Int. J. Non-Linear Mech.* **38**(7), 1053–1065 (2003)
  109. Duenas, T.A., Hsu, L., Cakman, G.P.: Magnetostrictive composite material systems analytical/experimental. *MRS Proc.* **459**, 527 (1996)
  110. Zheng, X.J., Sun, L.: A nonlinear constitutive model of magneto-thermo-mechanical coupling for giant magnetostrictive materials. *J. Appl. Phys.* **100**(6), 063906 (2006)
  111. Sun, L., Zheng, X.J.: Numerical simulation on coupling behavior of Terfenol-D rods. *Int. J. Solids Struct.* **43**(6), 1613–1623 (2006)
  112. Zheng, X.J., Sun, L.: A one-dimension coupled hysteresis model for giant magnetostrictive materials. *J. Magn. Magn. Mater.* **309**(2), 263–271 (2007)
  113. Jin, K., Kou, Y., Zheng, X.J.: A nonlinear magneto-thermo-elastic coupled hysteretic constitutive model for magnetostrictive alloys. *J. Magn. Magn. Mater.* **324**(12), 1954–1961 (2012)
  114. Jin, K., Kou, Y., Liang, Y.R., et al.: Effects of hysteresis losses on dynamic behavior of magnetostrictive actuators. *J. Appl. Phys.* **110**(9), 093908 (2011)
  115. Ewing, J.A.: *Magnetic induction in iron and other metals. The Electrician* (1900)
  116. Huang, B.Y.: Numerical simulation study of coupling between stress and magnetism for magnetic memory effect of the welding crack. Tianjin University, Tianjun (2007)
  117. Li, L.J., Wang, X.F., Yang, B.F., et al.: Simulation and experiment study of the ferromagnetic metal memory effect. *Nondestruct. Test.* **34**(12), 37–40 (2012)
  118. Li, X.M., Ding, H.S., Guo, G.M., et al.: Simulation of stress-magnetization effect for Q235 steel. *J. Test. Meas. Technol.* **27**(2), 167–173 (2013)

119. Li, Y., Ren, S.K.: Magnetization reversal of ferromagnetic specimens under the static tension conditions. *J. Iron Steel Res.* **25**(3), 30–33 (2013)
120. Ren, J.L., Shu, M.H., Song, K., et al.: Simulation of stress-magnetization effect on 18CrNi4A steel by ANSYS. *J. Mater. Eng.* **30**(11), 40–44 (2009)
121. Li, J.W., Xu, M.Q.: Modified Jiles-Atherton-Sablik model for asymmetry in magnetomechanical effect under tensile and compressive stress. *J. Appl. Phys.* **110**(6), 063918 (2011)
122. Wang, Z.D., Deng, B., Yao, K.: Physical model of plastic deformation on magnetization in ferromagnetic materials. *J. Appl. Phys.* **109**(8), 083928 (2011)
123. Yao, K., Shen, K., Wang, Z.D., et al.: Three-dimensional finite element analysis of residual magnetic field for ferromagnets under early damage. *J. Magn. Magn. Mater.* **354**, 112–118 (2014)
124. Bai, Y., Xu, F., Qiao, A.T.: Relationship between residual plastic deformation and metal magnetic memory signal and specimens. *J. Mater. Eng.* **3**(8), 42–49 (2013)
125. Avakian, A., Ricoeur, A.: An extended constitutive model for nonlinear reversible ferromagnetic behaviour under magnetomechanical multiaxial loading conditions. *J. Appl. Phys.* **121**(5), 053901 (2017)
126. Moonesan, M., Kashefi, M.: Effect of sample initial magnetic field on the metal magnetic memory NDT result. *J. Magn. Magn. Mater.* **460**, 285–291 (2018)
127. Libo, Wu, Kai, Y., Pengpeng, S., Bingxun, Z., Yuesheng, W.: Influence of inhomogeneous stress on biaxial 3D magnetic flux leakage signals. *NDT and E Int.* **108**, 102178 (2019)
128. Pengcheng, Z., Pengpeng, S., Ke, J., Xiaojing, Z.: A nonlinear anisotropic magneto-mechanical constitutive model and its application on magnetic memory testing method. *J. Appl. Phys.* **125**(22), 233901 (2019)
129. Yuan, J.J., Zhang, W.M., Liu, H.G., et al.: Influence of dynamic tension load on weak magnetic signals and metal magnetic memory effects of ferromagnetic samples. *Trans. Beijing Inst. Technol.* **26**(9), 785–788 (2006)
130. Yan, T.J., Zhang, J.D., Feng, G.D., et al.: Early inspection of wet steam generator tubes based on metal magnetic memory method. *Procedia Eng.* **15**(1), 1140–1144 (2011)
131. Duan, Z.X., Ren, S.K., Xi, X.W., et al.: Magnetizing reversal characteristic of 40Cr steel during stress-magnetizing process. *J. Iron Steel Res.* **28**(1), 77–80 (2016)
132. Shi, C.L., Dong, S.Y., Xu, B.S., et al.: Stress concentration degree affects spontaneous magnetic signals of ferromagnetic steel under dynamic tension load. *NDT&E Int.* **43**(1), 8–12 (2010)
133. Wang, H.P., Dong, L.H., Dong, S.Y., et al.: Fatigue damage evaluation by metal magnetic memory testing. *J. Cent South Univ.* **21**(1), 65–70 (2014)
134. Wang, H.T., Liu, P., Tian, G.Y., et al.: The accumulation mechanism of metal magnetic memory. *Nondestruct. Test.* **32**(9), 670–674 (2010)
135. Dong, L.H., Xu, B.S., Dong, S.Y., et al.: Metal magnetic memory testing for early damage assessment in ferromagnetic materials. *J. Cent South Univ. Technol.* **12**(S2), 102–106 (2005)
136. Dong, L.H., Xu, B.S., Dong, S.Y., et al.: Monitoring fatigue crack propagation of ferromagnetic materials with spontaneous abnormal magnetic signals. *Int. J. Fatigue* **30**(9), 1599–1605 (2008)
137. Shi, C.L., Tang, W.X., Zhan, H., et al.: Characterization of crack initiation life in ferromagnetic material by metal magnetic memory testing. *Mater. Sci. Forum* **817**(6), 791–796 (2015)
138. Chen, X., Li, L.M., Hu, B., et al.: Magnetic evaluation of fatigue damage in train axles without artificial excitation. *Insight Nondestruct. Test Condition Monitor* **48**(6), 342–345 (2006)
139. Leng, J.C., Zhang, H., Wang, L.H., et al.: Research of magnetic memory signal characteristics corresponding to early fatigue damage. *Int. J. Appl. Electromagn. Mech.* **46**(1), 143–154 (2014)
140. Xing, H.Y., Dang, Y.B., Wang, B., et al.: Quantitative metal magnetic memory reliability modeling for welded joints. *Chin. J. Mech. Eng.* **29**(2), 372–377 (2016)
141. Qian, Z.C., Huang, H.H., Jian, S.L., et al.: Research on magnetic memory signal of ferromagnetic material under tensile and compressive fatigue loading. *J. Electron Meas. Instrum.* **30**(4), 506–517 (2016)
142. Huang, H.H., Jiang, S.L., Wang, Y., et al.: Characterization of spontaneous magnetic signals induced by cyclic tensile stress in crack propagation stage. *J. Magn. Magn. Mater.* **365**(365), 70–75 (2014)
143. Huang, H.H., Yao, J.Y., Li, Z.W., et al.: Residual magnetic field variation induced by applied magnetic field and cyclic tensile stress. *NDT&E Int.* **63**(4), 38–42 (2014)
144. Huang, H.H., Han, G., Qian, Z.C., et al.: Characterizing the magnetic memory signals on the surface of plasma transferred arc cladding coating under fatigue loads. *J. Magn. Magn. Mater.* **443**, 281–286 (2017)
145. Li, C.C., Dong, L.H., Wang, H.D., et al.: Metal magnetic memory technique used to predict the fatigue crack propagation behavior of 0.45% C steel. *J. Magn. Magn. Mater.* **405**, 150–157 (2016)
146. Kolařík, K., Šimeček, J., Kříž, A., et al.: Using the Barkhausen-noise analysis and metal-magnetic-memory method for material characteristics under fatigue damage. *Materiali in Tehnologije* **51**(3), 437–441 (2017)
147. Li, Y.F., Zeng, X.G., Wei, L.M., et al.: Characterizations of damage-induced magnetization for X80 pipeline steel by metal magnetic memory testing. *Int. J. Appl. Electromagn. Mech.* **54**(1), 1–13 (2017)
148. Hu, B., Chen, G., Shen, G.T., et al.: Study on magnetic memory method (MMM) for fatigue evaluation. *Proc. 17th World Conference on Nondestructive Testing* 25–28 (2008)
149. Huang, H.H., Jiang, S.L., Liu, R.J., et al.: Investigation of magnetic memory signals induced by dynamic bending load in fatigue crack propagation process of structural steel. *J. Nondestruct. Eval.* **33**(3), 407–412 (2014)
150. Huang, H.H., Qian, Z.C., Yang, C., et al.: Magnetic memory signals of ferromagnetic weldment induced by dynamic bending load. *Nondestruct. Test Eval.* **32**(2), 166–184 (2017)
151. Leng, J.C., Xu, M.X., Xu, M.Q., et al.: Magnetic field variation induced by cyclic bending stress. *NDT&E Int.* **42**(5), 410–414 (2009)
152. Xu, M.X., Xu, M.Q., Li, J.W., et al.: Metal magnetic memory field characterization at early fatigue damage based on modified Jiles-Atherton model. *J. Cent. South Univ.* **19**(6), 1488–1496 (2012)
153. Xu, M.X., Chen, Z.H., Xu, M.Q.: Micro-mechanism of metal magnetic memory signal variation during fatigue. *Int. J. Min. Met. Mater.* **21**(3), 259–265 (2014)
154. Li, J.W., Zhong, S., Lv, G.P., et al.: The variation of surface magnetic field induced by fatigue stress. *J. Nondestruct. Eval.* **32**(3), 238–241 (2013)
155. Hu, Z.B., Fan, J.C., Wu, S.N., et al.: Characteristics of metal magnetic memory testing of 35CrMo steel during fatigue loading. *Metals* **8**(2), 119 (2018)
156. Qian, Z.C., Huang, H.H., Liu, W.J., et al.: Magnetomechanical model for coating/substrate interface and its application in interfacial crack propagation length characterization. *J. Appl. Phys.* **124**(20), 203904 (2018)
157. Qian, Z.C., Huang, H.H.: Coupling fatigue cohesive zone and magnetomechanical model for crack detection in coating interface. *NDT and E Int.* **105**, 25–34 (2019)

158. Guralnick, S.A., Bao, S., Erber, T.: Piezomagnetism and fatigue: II. *J. Phys. D* **41**(11), 115006 (2008)
159. Bao, S., Jin, W.L., Huang, M.F., et al.: Piezomagnetic hysteresis as a non-destructive measure of the metal fatigue process. *NDT&E Int.* **43**(8), 706–712 (2010)
160. Bao, S., Erber, T., Guralnick, S.A., et al.: Fatigue, magnetic and mechanical hysteresis. *Strain* **47**(4), 372–381 (2011)
161. Bao, S., Gong, S.F.: Magnetomechanical behavior for assessment of fatigue process in ferromagnetic steel. *J. Appl. Phys.* **112**(11), 113902 (2012)
162. Bao, S., Wang, J.: Magnetomechanical measurements for nondestructive evaluation of failure in steel structural element. *J. Mater. Eng. Perform.* **22**(5), 1351–1354 (2013)
163. Bao, S., Fu, M.L., Gu, Y., et al.: Evolution of the piezomagnetic field of ferromagnetic steel subjected to cyclic tensile stress with variable amplitudes. *Exper Mech.* **56**(6), 1017–1028 (2016)
164. Chen, Z.M., Aoto, K., Kato, S.: Passive electromagnetic NDE for mechanical damage inspection by detecting leakage magnetic flux. *Japan Nuclear Cycle Development Inst* (1999).
165. Chen, Z.M., Aoto, K., Miya, K.: NDE of fatigue damage in austenitic stainless steel by measuring and inversion of damage-induced magnetic field. In: Kojima, F., Takagi, T., Udpa, T., Pavo, J. (eds.) *Electromagnetic Nondestructive Evaluation* 127–134 (2002)
166. Li, H.M., Chen, Z.M., Li, Y.: Characterization of damage-induced magnetization for 304 austenitic stainless steel. *J. Appl. Phys.* **110**(11), 114907 (2011)
167. Li, H.M., Chen, Z.M., Li, Y., et al.: Dependence of deformation-induced magnetic field on plastic deformation for SUS304 stainless steel. *Int. J. Appl. Electromagn. Mech.* **38**(1), 17–26 (2012)
168. Bai, P.G., Shi, P.P., Zhao, Y.S., Chen, H.E., Xie, S.J., Chen, Z.M.: Joint effect of residual stress and plastic deformation on pulsed eddy current response signals in 304 austenitic stainless steel. *Int. J. Appl. Electromagn. Mech.* (2019). <https://doi.org/10.3233/JAE-190124>
169. Yan, C.Y., Li, W.S., Di, X.J., et al.: Variation regularity of metal magnetic memory signals with inspecting time-interval and location. *J. Cent. South Univ.* **14**(3), 319–323 (2007)
170. Zhong, L.Q., Li, L.M., Chen, X.: Magnetic signals of stress concentration detected in different magnetic environment. *Nondestruct. Test Eval.* **25**(2), 161–168 (2010)
171. Hu, B., Li, L., Chen, X., et al.: Study on the influencing factors of magnetic memory method. *Int. J. Appl. Electromagn. Mech.* **33**(3–4), 1351–1357 (2010)
172. Bao, S., Hu, S.N., Lin, L., et al.: Experiment on the relationship between the magnetic field variation and tensile stress considering the loading history in U75V rail steel. *Insight Nondestruct. Test Condition Monitor* **57**(12), 683–688 (2015)
173. Bao, S., Zhang, D.: The effect of loading speed on the residual magnetic field of ferromagnetic steel subjected to tensile stress. *Insight Nondestruct. Test Condition Monitor* **57**(7), 401–405 (2015)
174. Huang, H.H., Qian, Z.C.: Effect of temperature and stress on residual magnetic signals in ferromagnetic structural steel. *IEEE Trans. Magn.* **53**(1), 1–8 (2017)
175. Xu, K.S., Qiu, X.Q., Tian, X.S.: Investigation of metal magnetic memory signals of welding cracks. *J. Nondestruct. Eval.* **36**(2), 20 (2017)
176. Singh, W.S., Stegemann, R., Kreuzbruck, M., et al.: Mapping of deformation-induced magnetic fields in carbon steels using a GMR sensor based metal magnetic memory technique. *J. Nondestruct. Eval.* **37**(2), 21 (2018)
177. Sun, Y., Liu, S., Ye, Z., et al.: A defect evaluation methodology based on multiple magnetic flux leakage (MFL) testing signal eigenvalues. *Res. Nondestruct. Eval.* **27**(1), 1–25 (2016)
178. Ramuhalli, P., Udpa, L., Udpa, S.S.: Electromagnetic NDE signal inversion by function-approximation neural networks. *IEEE Trans. Magn.* **38**(6), 3633–3642 (2002)
179. Kishimoto, M., Sakasai, K., Ara, K.: Solution of electromagnetic inverse problem using combinational method of Hopfield neural network and genetic algorithm. *J. Appl. Phys.* **79**(1), 1–7 (1996)
180. Khodayari-Rostamabad, A., Reilly, J.P., Nikolova, N.K., et al.: Machine learning techniques for the analysis of magnetic flux leakage images in pipeline inspection. *IEEE Trans. Magn.* **45**(8), 3073–3084 (2009)
181. Hari, K.C., Nabi, M., Kulkarni, S.V.: Improved FEM model for defect-shape construction from MFL signal by using genetic algorithm. *IET Sci. Meas. Technol.* **1**(4), 196–200 (2007)
182. Khan, T., Ramuhalli, P.: A recursive bayesian estimation method for solving electromagnetic nondestructive evaluation inverse problems. *IEEE Trans. Magn.* **44**(7), 1845–1855 (2008)
183. Zhang, Y., Ye, Z.F., Wang, C.: A fast method for rectangular crack sizes reconstruction in magnetic flux leakage testing. *NDT&E Int.* **42**(5), 369–375 (2009)
184. Han, W., Xu, J., Wang, P., et al.: Defect profile estimation from magnetic flux leakage signal via efficient managing particle swarm optimization. *Sensors* **14**(6), 10361–10380 (2014)
185. Cai, C., Rodet, T., Lambert, M.: Influence of partially known parameter on flaw characterization in eddy current testing by using a random walk MCMC method based on metamodeling. *J. Phys. Conf. Ser.* **542**(1), 012009 (2014)
186. Priewald, R.H., Magele, C., Ledger, P.D., et al.: Fast magnetic flux leakage signal inversion for the reconstruction of arbitrary defect profiles in steel using finite elements. *IEEE Trans. Magn.* **49**(1), 506–516 (2013)
187. Chen, Z.M., Miya, K.: ECT inversion using a knowledge-based forward solver. *J. Nondestruct. Eval.* **17**(3), 167–175 (1998)
188. Chen, Z.M., Aoto, K., Miya, K.: Reconstruction of cracks with physical closure from signals of eddy current testing. *IEEE Trans. Magn.* **36**(4), 1018–1022 (2000)
189. Chen, Z.M., Preda, G., Mihalache, O., et al.: Reconstruction of crack shapes from the MFLT signals by using a rapid forward solver and an optimization approach. *IEEE Trans. Magn.* **38**(2), 1025–1028 (2002)
190. Rebican, M., Chen, Z.M., Yusa, N., et al.: Shape reconstruction of multiple cracks from ECT signals by means of a stochastic method. *IEEE Trans. Magn.* **42**(4), 1079–1082 (2006)
191. Xie, S.J., Chen, Z.M., Toshiyuki, T., et al.: Quantitative non-destructive evaluation of wall thinning defect in double-layer pipe of nuclear power plants using pulsed ECT method. *NDT&E Int.* **75**, 87–95 (2015)
192. Dubov, A.A.: Diagnostics of steam turbine disks using the metal magnetic memory method. *Therm. Eng.* **57**(1), 16–21 (2010)
193. Dubov, A., Demin, E., Milyaev, A., et al.: The experience of gas pipeline stress-strain state control with usage of the metal magnetic memory method as compared with conventional methods and stress control means. *Weld. World* **46**(9–10), 29–33 (2002)
194. Dubov, A., Kolokolnikov, S.: Comprehensive diagnostics of parent metal and welded joints of steam pipeline bends. *Weld. World* **54**(9/10), 241–248 (2010)
195. Dubov, A., Kolokolnikov, S.: Assessment of the material state of oil and gas pipelines based on the metal magnetic memory method. *Weld. World* **56**(3–4), 11–19 (2012)
196. Li, C., Chen, C., Liao, K.: A quantitative study of signal characteristics of non-contact pipeline magnetic testing. *Insight-Nondestructive Test. Condit. Monitor.* **57**(6), 324–330 (2015)
197. Liu, B., Ma, Z., Liu, Z., et al.: Research on internal detection technology for axial crack of long-distance oil and gas pipeline based on micromagnetic method. *Struct. Health Monitor.* (2019). <https://doi.org/10.1177/1475921719877361>

198. Liu, B., He, L., Ma, Z., Zhang, H., Sfarra, S., Fernandes, H., Perilli, S.: Study on internal stress damage detection in long-distance oil and gas pipelines via weak magnetic method. *ISA Trans.* **89**, 272–280 (2019)
199. Liu, B., He, L., Zhang, H., Sfarra, S., Fernandes, H., Perilli, S., Ren, J.: Research on stress detection technology of long-distance pipeline applying non-magnetic saturation. *IET Sci. Meas. Technol.* **13**(2), 168–174 (2019)
200. Chenhui, K., et al.: Experiment research on the metal magnetic memory in gear micro crack detection. Proceedings of the 2011 IEEE International Conference on Mechatronics and Automation, August 7–10, Beijing, China
201. Roskosz, M., Rusin, A., Kotowicz, J.: The metal magnetic memory method in the diagnostics of power machinery component. *J. Achiev. Mater. Manuf. Eng.* **1**, 362–370 (2010)
202. Roskosz, M.: Application of the metal magnetic memory method for the inspection of teeth in toothed wheels. *Tech. Inspect.* **1**, 15–20 (2006)
203. Roskosz M. Possibilities of the application of the metal magnetic memory method to the analysis of gear durability. Proceedings of the 9th European Conference on Non-Destructive Testing ECNDT, Berlin, 2006.
204. Dubov, A., Kolokolnikov, S.: Application of the metal magnetic memory method for detection of defects at the initial stage of their development for prevention of failures of power engineering welded steel structures and steam turbine parts. *Weld. World* **58**(2), 225–236 (2014)
205. Dubov, A., Kolokolnikov, S.: The metal magnetic memory method application for online monitoring of damage development in steel pipes and welded joints specimens. *Weld. World* **57**, 123–136 (2013)
206. Li, L.M., Huang, S.L., Wang, X.F., Shi, K.R., Wu, S.: Magnetic field abnormality caused by welding residual stress. *J. Magn. Mater.* **261**, 385–391 (2003)
207. Li, W.S., Di, X.J., Bai, S.W., Liu, F.M., Xue, Z.K.: Feature analysis of metal magnetic memory signals for weld cracking-based on wavelet energy spectrum. *Insight-Non-Destruct. Test. Condition Monitor.* **48**(7), 426–429 (2006)
208. Yang, Y., Su, S., Wang, W., Ma, X.P., Hu, J.Y.: Comparative study on the characteristics of magnetic memory signals for welding and non-welding steels with different materials under tension-compression fatigue. *Int. J. Appl. Electromagnet. Mech.* (2020). <https://doi.org/10.3233/JAE-190064>
209. Xin, Qi, Shu, Di, Hui, L., Wei, W., Chen, J.: Magnetic Barkhausen noise, metal magnetic memory testing and estimation of the ship plate welded structure stress. *J. Nondestruct. Eval.* **31**(1), 80–89 (2012)
210. Su, S., Zhao, X.R., Wang, W., Zhang, X.H.: Metal magnetic memory inspection of Q345 steel specimens with butt weld in tensile and bending test. *J. Nondestruct. Eval.* **38**, 64 (2019). <https://doi.org/10.1007/s10921-019-0603-8>
211. Agnieszka, K.-S., Smoczek, J., Szytko, J.: Crane frame inspection using metal magnetic memory method. *J. KONES* **23**(2), 185–192 (2016)
212. Wang, W., Yi, S.C., Su, S.Q.: Experimental investigation of stress and damage characterization of steel beam buckling using magnetic memory signals. *Struct. Des. Tall Special Build.* **25**(11), 505–518 (2016)
213. Su, S.Q., Wei, L.X., Wang, W., Yang, Y.Y., Ma, X.P., Zuo, F.L.: Equivalent stress for steel box girder with corrugated web under bending based on magnetic memory method. *Int. J. Appl. Electromagnet. Mech.* (2020). <https://doi.org/10.3233/JAE-190075>
214. Dong, L.H., Xu, B.S., Xue, N., Wang, H.P., Lin, H.Y.: Development of remaining life prediction of crankshaft remanufacturing core. *Adv. Manuf.* **1**, 91–96 (2013)
215. Lesiak, P., Radziszewski, A.: Application of the metal magnetic memory method in rail transport. *Tech. Inspect.* **2**, 32–39 (2005)
216. Lesiak, P., Radziszewski, A.: Rail diagnostics with the use of the metal magnetic memory method. *Scientific Works of the Technical University of Radom, Electrics* **2**(8), 103–110 (2004)

**Publisher's Note** Springer Nature remains neutral with regard to jurisdictional claims in published maps and institutional affiliations.